

# Non-equilibrium cotunneling in quantum dot Josephson junctions

Jordi Picó-Cortés,<sup>1,2</sup> Gloria Platero,<sup>2</sup> Andrea Donarini,<sup>1</sup> and Milena Grifoni<sup>1</sup>

<sup>1</sup>*Institute for Theoretical Physics, University of Regensburg, 93040 Regensburg, Germany.*

<sup>2</sup>*Instituto de Ciencia de Materiales de Madrid (CSIC) 28049 Madrid, Spain.*

We investigate non-equilibrium transport through superconducting nanojunctions using a Liouville space approach. The formalism allows us to study finite gap effects, and to account for both quasiparticle and Cooper pair tunneling. With focus on the weak tunneling limit, we study the stationary dc and ac current up to second order (cotunneling) in the hybridization energy. For the particular case of a strongly interacting quantum dot sandwiched between two superconductors, we identify the characteristic virtual processes that yield the Andreev and Josephson current and obtain the dependence on the gate and bias voltage for the dc current, the critical current and the phase-dependent dissipative current. In particular, the critical current is characterized by regions in the stability diagram in which its sign changes from positive to negative, resulting in a multitude of  $0 - \pi$  transitions. The latter signal the interplay between strong interactions and tunneling at finite bias.

## I. INTRODUCTION

Advancements in nanostructure fabrication have allowed the manufacturing of increasingly smaller Josephson junctions. For mesoscopic and nano-sized junctions, genuine quantum mechanical effects often rule the transport properties of the device. Superconducting junctions based on quantum point contacts were among the first of such systems to be studied in detail [1–3]. For short weak links with few channels, multiple coherent Andreev reflections give rise to current-carrying Andreev bound states which can be employed to effectively characterize the properties of the Josephson current [4]. These ideas have been used extensively in recent years to investigate novel superconducting transport phenomena, such as the fractional Josephson effect in topological junctions [5–7], non-reciprocal transport [8–10], and multi-terminal junctions [11, 12].

As the size of the junction is decreased even further, Coulomb interaction effects between the strongly confined charge carriers becomes more important. Josephson junctions based on quantum dots (QDs), have been studied in detail both experimentally [13–17] and theoretically [18–20]. They have further received attention as a platform for quantum computation, in the form of Andreev spin qubits [21, 22]. The combination of superconducting correlations and electronic interactions yields a rich phenomenology [23, 24]. A hallmark of this interplay is the  $0 - \pi$  transition, occurring in QDs with odd occupancy. Here the sign of the equilibrium critical current changes as the junction’s ground state turns from a singlet to a doublet [25–29]. For strongly coupled QDs, Kondo correlations further affect the doublet and singlet phases [30–33]. This work extends these results to a non-equilibrium situation. In particular, we show that a multitude of  $0 - \pi$  transitions can be observed in weakly coupled junctions, in a delicate interplay between interaction effects and Cooper pair tunneling at finite bias.

The Green’s function formalism is the method of choice for non-interacting junctions. While it has been extended to interacting systems via mean field [34, 35] and per-

turbative expansions [36, 37], the regime of interest for Josephson junctions often involves interaction strengths that lie beyond the applicability of these approximation schemes [38]. Alternatively, the tunnel coupling to the leads can be treated perturbatively while keeping the interaction exactly [39–41]. In order to perform this expansion systematically, a generalized master equation (GME) for the density operator can be employed [42–44], in which the distinct tunneling processes can be identified using diagrammatic techniques. This formalism can furthermore be extended to larger tunneling amplitudes via diagrammatic resummations [45–47] and renormalization group methods [48].

The GME approach has found applications in the study of QD-based Josephson junctions. This includes three-terminal junctions with one non superconducting lead which acts as a tunneling probe [49–51], Cooper pair splitters [52–55] and Andreev bound state spectra [15, 56, 57]. Many of these works employ other approximations on top of weak coupling, such as the assumption of infinite gap or infinite interaction. The former, in particular, allows for resummation techniques that restore the Andreev bound state picture [58–60], and can even be extended to capture perturbatively the effect of the quasiparticles [61]. Recent works have employed fermionic duality to investigate the dynamics in the time domain of junctions with large gap superconductors [62, 63].

Non-equilibrium properties of Josephson junctions through interacting quantum dots have received a comparatively poor attention so far. This regime offers, nonetheless, a rich phenomenology [64–69]. The finite bias properties of a carbon-nanotube based Josephson QD have been probed in a recent experiment by the measurement of the Josephson radiation [70] with intriguing unexplained features. This is the topic of the present work.

In the non-equilibrium case the GME approach is often used in a particle conserving framework of superconductivity [71], since it naturally allows to account for finite bias voltages across the junction [49, 67]. In a recent

publication [72], some of us have employed the GME approach to investigate the interplay of a dc and an ac bias voltage on the transport characteristics of a Josephson quantum dot at finite gaps, temperature and interaction. In that study it was shown that, already in lowest order in the tunneling coupling, intriguing features may occur, such as an inversion of the dc-current due to the combination of the ac drive and a non-flat density of states.

Here we focus solely on the effects of a dc voltage bias on transport and fully include the first two non-vanishing orders in the tunnel coupling. We provide comprehensive numerical and analytical results for both the dc component of the current as well as its first harmonic in the ac Josephson frequency. For the latter, which provides the Josephson current out of equilibrium, we find two distinct contributions: the critical current, which may be non-zero at zero bias, and a phase-dependent dissipative term, sometimes referred to as the  $\cos\varphi$  term [73, 74]. Knowledge of both allows us to evaluate the Josephson radiation, hence providing a direct benchmark to present cutting-edge experiments [70, 75].

As we shall see, accounting for the second order is fundamental, as the Josephson current is of this order for most situations. Inspection of the stability diagrams allows us to identify the relevant transport processes, being mediated solely by quasiparticles, Cooper pairs or a combination of both. For example, subgap features from thermally excited quasiparticles permeate the dc-component of the current. Cotunneling-like processes are responsible for a  $\pi$ -phase of the critical current in the odd Coulomb diamond at low bias, extending results found for the zero bias case [39].

The manuscript is organized as follows. Section II introduces the model and the transport theory that we will employ throughout this work. In particular, in Section II E we show how the ac Josephson effect appears naturally in the system as a consequence of considering arbitrary coherences involving Cooper pairs. In Section III we introduce the perturbative scheme employed to calculate the steady state density operator and the current. In Section IV and Section V we present numerical results for the dc and ac components of the current and highlight their main features. Finally, in Section VI we summarize our results and provide an outlook for future research.

## II. THEORETICAL FRAMEWORK

### A. Model Hamiltonian

We focus on the archetypal model of an interacting Josephson junction: the single impurity Anderson model (SIAM) with superconducting leads. The total Hamiltonian  $\hat{H} = \hat{H}_{SC} + \hat{H}_{QD} + \hat{H}_T$  includes the contributions from the leads  $\hat{H}_{SC}$ , the quantum dot  $\hat{H}_{QD}$ , and the tunnel coupling between them  $\hat{H}_T$ . The last two are

given respectively by

$$\hat{H}_{QD} = \sum_{\sigma} \epsilon_d \hat{d}_{\sigma}^{\dagger} \hat{d}_{\sigma} + U \hat{d}_{\uparrow}^{\dagger} \hat{d}_{\downarrow}^{\dagger} \hat{d}_{\downarrow} \hat{d}_{\uparrow}, \quad (1)$$

$$\hat{H}_T = \sum_{l\mathbf{k}\sigma} \left( t_{l\mathbf{k}} \hat{c}_{l\mathbf{k}\sigma}^{\dagger} \hat{d}_{\sigma} + t_{l\mathbf{k}}^* \hat{d}_{\sigma}^{\dagger} \hat{c}_{l\mathbf{k}\sigma} \right). \quad (2)$$

Here,  $\hat{d}_{\sigma}^{(\dagger)}$  are annihilation (creation) operators of the dot with spin  $\sigma = \uparrow, \downarrow$ , while  $\epsilon_d$  is the single particle energy of the dot, tunable via an electric gate with voltage  $V_g$ . We choose in the following  $\epsilon_d = -eV_g$ . Finally,  $U$  is the Coulomb interaction. The tunneling process is characterized by spin conserving tunneling amplitudes  $t_{l\mathbf{k}}$  for the transfer of a dot electron to lead  $l = L, R$ , where it is described by annihilation (creation) fermionic operators  $\hat{c}_{l\mathbf{k}\sigma}^{(\dagger)}$  with momentum  $\mathbf{k}$  and spin  $\sigma$ .

In order to account for charge transfer out of equilibrium, we treat the superconductors in a particle-conserving formulation [76, 77]. In this framework, the bare fermion operators can be written, employing the particle-conserving Bogoliubov-Valatin transformations, as

$$\hat{c}_{l\mathbf{k}\sigma}^{\dagger} = u_{l\mathbf{k}} \hat{\gamma}_{l\mathbf{k}\sigma}^{\dagger} + \sigma v_{l\mathbf{k}}^* \hat{\gamma}_{l\mathbf{k}\bar{\sigma}} \hat{S}_l^{\dagger}, \quad (3)$$

where  $\sigma = \pm$  for  $\uparrow / \downarrow$ , respectively, and

$$u_{l\mathbf{k}} = \sqrt{(1/2) (1 + \xi_{l\mathbf{k}}/E_{l\mathbf{k}})}, \quad (4)$$

$$v_{l\mathbf{k}} = e^{i\phi_l} \sqrt{(1/2) (1 - \xi_{l\mathbf{k}}/E_{l\mathbf{k}})}, \quad (5)$$

with  $E_{l\mathbf{k}} = \sqrt{\xi_{l\mathbf{k}}^2 + |\Delta_l|^2}$  the quasiparticle excitation energy for mode  $\mathbf{k}$ . Here,  $\xi_{l\mathbf{k}}$  describes the single particle dispersion of the bare fermions measured from the chemical potential  $\mu_l$ ,  $\Delta_l$  is the superconducting order parameter, and  $\phi_l = \arg(\Delta_l)$ . We take  $\phi_l = 0$  in this work without loss of generality. More importantly, we have employed the Bogoliubov operators  $\hat{\gamma}_{l\mathbf{k}\sigma}^{\dagger}, \hat{\gamma}_{l\mathbf{k}\sigma}$  which describe quasiparticle excitations, as well as Cooper pair operators  $\hat{S}_l, \hat{S}_l^{\dagger}$  which destroy or create a Cooper pair in the condensate [71]. Hence, the Bogoliubov-Valatin transformation conserves the total charge. The first term in Eq. (3) describes an electron-like excitation, while the second is associated with a hole-like excitation [78].

The quasiparticle states are characterized by the occupation  $\nu_{l\mathbf{k}\sigma} = 0, 1$  of the fermionic modes, and the state of the Cooper pair condensate by the total number of Cooper pairs, which we denote by  $M_l$ . With this, we can write an arbitrary state of lead  $l$  as  $|M_l\rangle |\{\nu_{l\mathbf{k}\sigma}\}\rangle$ , with total number of electrons (Cooper pairs and quasiparticles) equal to  $N_l = 2M_l + \sum_{\mathbf{k}\sigma} \nu_{l\mathbf{k}\sigma}$ . The effect of the Cooper pair operators on any such state is given by

$$\hat{S}_l^{\dagger} |M_l\rangle |\{\nu_{l\mathbf{k}\sigma}\}\rangle = |M_l + 1\rangle |\{\nu_{l\mathbf{k}\sigma}\}\rangle. \quad (6)$$

Similarly,  $\hat{S}_l$  reduces  $M_l$  by 1 and leaves the occupation of the quasiparticle states invariant. Employing this, we

see that the Cooper pair and quasiparticle operators commute [79]

$$[\hat{S}_l^\dagger, \hat{\gamma}_{lk\sigma}^\dagger] = [\hat{S}_l^\dagger, \hat{\gamma}_{lk\sigma}] = 0. \quad (7)$$

Moreover, the Cooper pair creation and annihilation operators satisfy

$$\hat{S}_l \hat{S}_l^\dagger = 1, \quad [\hat{S}_l, \hat{S}_l^\dagger] \propto \mathcal{O}(1/M_l). \quad (8)$$

Assuming that the Cooper pair operators commute is a good approximation in the limit of large Cooper pair numbers and we do so from here onward.

Upon employing Eq. (3), we can divide the Hamiltonian for the leads into two contributions,  $\hat{H}_{SC} = \hat{H}_{QP} + \hat{H}_{CP}$ . The former describes the quasiparticle excitations and reads

$$\hat{H}_{QP} = \sum_{lk\sigma} E_{lk} \hat{\gamma}_{lk\sigma}^\dagger \hat{\gamma}_{lk\sigma} + \sum_l \mu_l \hat{N}_{QP,l}, \quad (9)$$

$$\hat{N}_{QP,l} = \sum_{k\sigma} \hat{\gamma}_{lk\sigma}^\dagger \hat{\gamma}_{lk\sigma}, \quad (10)$$

where  $\mu_l = a_l e V_b$  is the chemical potential of lead  $l$ ,  $V_b$  is the bias voltage and the coefficients  $a_l$  satisfy  $a_L - a_R = 1$ . The latter contribution  $\hat{H}_{CP}$  describes the Cooper pair condensate and has the form

$$\hat{H}_{CP} = \sum_l \mu_l \hat{N}_{CP,l}, \quad \hat{N}_{CP,l} |M_l\rangle = 2M_l |M_l\rangle. \quad (11)$$

Together with Eq. (6) and the corresponding equation for  $\hat{S}_l$ , it follows that  $[\hat{S}_l, \hat{H}_{CP}] = 2\mu_l \hat{S}_l$ .

The Hamiltonian  $\hat{H}_{SC}$  corresponds to a mean field approximation to the true Hamiltonian of the superconductor. By definition, the quasiparticles operators describe excitations on top of the ground state. Within the mean field approximation, the quasiparticle spectrum is assumed to be independent of the number of Cooper pairs in the ground state, yielding the commutation relations in Eq. (7). As a result of these relations, we find  $[\hat{S}_l, \hat{H}_T] \sim [\hat{S}_l, \hat{S}_l^\dagger] \sim 0$  in the approximation of large Cooper pair numbers, but  $[\hat{H}_T, \hat{N}_{CP}] \neq 0$ . The consequences and validity of the approximation will be further discussed in Section II E. We anticipate that, since the quasiparticles are the only source of dissipation in the model, the dynamics of the Cooper pair operators are completely coherent and their time evolution is fully determined by the Cooper pair Hamiltonian.

## B. Transport theory

Interacting open quantum systems can be studied via a many-body generalized master equation (GME) based on the Nakajima-Zwanzig formalism [80, 81]. The GME describes the dynamics of a central system (denoted by  $S$  from here on) under the effect of the coupling to a bath

(denoted by  $B$ ). In the context of transport, the system is often considered to be the nanostructure through which the current flows (in this case, the quantum dot) and the bath the electrodes to which it is coupled. However, we note that the distinction between ‘‘system’’ and ‘‘bath’’ is, in the Nakajima-Zwanzig formalism, purely one of convenience. Indeed, we will make use of this fact shortly in order to account for the peculiarities of the superconducting case.

We define the reduced density operator as  $\hat{\rho}_S(t) = \text{Tr}_B \{\hat{\rho}(t)\}$ , where  $\text{Tr}_k \{\dots\}$  indicates partial trace over subsystem  $k$ , and  $\hat{\rho}(t)$  is the density operator of the coupled bath and system; it satisfies the Liouville-von Neumann equation. The reduced density operator in turn obeys the GME [42–44]

$$\frac{d}{dt} \hat{\rho}_S(t) = \mathcal{L}_S \hat{\rho}_S(t) + \int_0^t ds \mathcal{K}_S(t-s) \hat{\rho}_S(s), \quad (12)$$

where  $i\hbar \mathcal{L}_k \hat{O} = [\hat{H}_k, \hat{O}]$  is the Liouvillian superoperator associated with the Hamiltonian  $\hat{H}_k$  and  $\mathcal{K}_S(t)$  is the propagation kernel. The first term on the right hand side fully encodes the coherent dynamics of the isolated system via  $\mathcal{L}_S$ , and the second the effect of the bath and its coupling to the system exactly via  $\mathcal{K}_S(t)$ .

Once the reduced density operator is known, the current through the junction can be calculated as the statistical average of the current operator. For lead  $l$ , this is given by  $\hat{I}_{l,H}(t) = -e d\hat{N}_{l,H}(t)/dt$ , with  $\hat{O}_{l,H}(t)$  referring to the Heisenberg picture representation of operator  $\hat{O}_l$ . Notice that  $\hat{N}_l$  accounts for both Cooper pairs and quasiparticles. Here and onward we consider the symmetrized current  $\hat{I} = (1/2)(\hat{I}_L - \hat{I}_R)$ . This expression avoids the issue of displacement currents [67, 82] which appear in time-dependent problems. Then, the statistical average of the current operator can be calculated as

$$I(t) = \langle \hat{I}(t) \rangle = \text{Tr}_S \left\{ \int_0^t ds \mathcal{J}_S(t-s) \hat{\rho}_S(s) \right\}, \quad (13)$$

where  $\mathcal{J}_S(t-s)$  is the current kernel. Both  $\mathcal{K}_S(t-s)$  and  $\mathcal{J}_S(t-s)$  are superoperators acting on the system degrees of freedom only. Their expressions are given in Appendix A.

## C. The stationary state

In the following, we focus on the stationary dynamics of the problem at  $t \rightarrow \infty$ . We start by considering solutions of Eq. (12) of the form

$$\hat{\rho}_S(t) = \sum_{\lambda_i} e^{\lambda_i t} \hat{r}_S(\lambda_i), \quad (14)$$

$$\hat{r}_S(\lambda_i) = \lim_{\lambda \rightarrow \lambda_i} (\lambda - \lambda_i) \text{L}\{\hat{\rho}_S\}(\lambda), \quad (15)$$

where  $\text{L}\{f\}(\lambda) = \int_0^\infty dt e^{-\lambda t} f(t)$  is the Laplace transform of  $f(t)$ . The residue operators  $\hat{r}_S(\lambda_i)$  with

$\text{Re}\{\lambda_i\} > 0$  in Eq. (14) are unphysical and those with  $\text{Re}\{\lambda_i\} < 0$  are transients which vanish in the stationary state. As such, we will only be concerned with the solutions satisfying  $\text{Re}\{\lambda_i\} = 0$ . Hermiticity of the density operator requires that for each  $\lambda_i$  its complex conjugate  $\lambda_i^*$  must also appear in Eq. (14), with  $\hat{r}_S(\lambda_i^*) = \hat{r}_S^\dagger(\lambda_i)$ . Furthermore,  $\lambda_i = 0$  must always be a solution in order to satisfy conservation of probability at all times. By the same reason it follows that  $\text{Tr}_S\{\hat{r}_S(\lambda_i)\} = \delta_{\lambda_i,0}$ .

The  $\hat{r}_S(\lambda_i)$  in Eq. (14) are the solutions of the equation

$$[\mathcal{L}_S - \lambda + \tilde{\mathcal{K}}_S(\lambda)]\hat{r}_S(\lambda) = 0. \quad (16)$$

Here, we use the short-hand notation  $\tilde{\mathcal{K}}_S(\lambda) \equiv \mathcal{L}\{\mathcal{K}_S\}(\lambda)$  for the Laplace transform of  $\mathcal{K}_S(t)$ , given by (see Appendix A)

$$\begin{aligned} \tilde{\mathcal{K}}_S(\lambda) \bullet = & \quad (17) \\ \text{Tr}_B \left\{ \mathcal{L}_T \sum_{k=0}^{\infty} (\tilde{\mathcal{G}}_0(\lambda) \mathcal{Q} \mathcal{L}_T \mathcal{Q})^{2k} \tilde{\mathcal{G}}_0(\lambda) \mathcal{L}_T \bullet \otimes \hat{\rho}_B \right\}, \end{aligned}$$

where we introduced the projector  $\mathcal{Q} \bullet = \bullet - \text{Tr}_B\{\bullet\} \otimes \hat{\rho}_B$ , with  $\hat{\rho}_B$  a reference density operator of the bath that satisfies  $\mathcal{L}_B \hat{\rho}_B = 0$ , and the Laplace-transformed free propagator

$$\tilde{\mathcal{G}}_0(\lambda) = \frac{1}{\lambda - \mathcal{L}_S - \mathcal{L}_B}. \quad (18)$$

The superoperator  $\tilde{\mathcal{K}}_S(\lambda)$  exists provided that  $\mathcal{K}_S(t)$  is bounded for  $t > 0$ , which we assume in the following. We remark that only even factors of the tunneling amplitude appear in Eq. (17) due to conservation of particle number and the overall trace over the quasiparticle bath.

The exponents  $\lambda_i$  appearing in Eq. (14) are the solutions of a non-linear eigenvalue equation, which can be hard to find even for simple systems. In the case of a Josephson quantum dot, symmetry arguments allow one to obtain exactly the subset of eigenvalues  $\{\lambda_i\}$  governing the stationary dynamics, as we will show in Section II E.

The current for a solution of the form of Eq. (16) can be obtained via

$$I(t) = \sum_{\lambda_i} \text{Tr}_S \left\{ \tilde{\mathcal{J}}_S(\lambda_i) \hat{r}_S(\lambda_i) \right\} e^{\lambda_i t}, \quad (19)$$

with  $\tilde{\mathcal{J}}_S(\lambda)$  the Laplace-transformed current kernel, resulting from substituting the leftmost instance of  $\mathcal{L}_T$  for the current operator  $\hat{I}$  in Eq. (17).

#### D. Transport equations for a Josephson junction

We now turn to the question of dealing with the Cooper pair degrees of freedom within the transport theory outlined above. Within the mean field description introduced in Section II A, the quasiparticles are fermionic excitations of the superconductor on top of a Cooper pair

condensate. It is thus natural to view the quasiparticles as the environment and the Cooper pairs as part of the system [49]. We therefore take in the following

$$\hat{H}_S = \hat{H}_{QD} + \hat{H}_{CP}, \quad \hat{H}_B = \hat{H}_{QP}, \quad (20)$$

with the reference density operator  $\hat{\rho}_B$  [entering in Eq. (17)] chosen to be the equilibrium density operator of the quasiparticles only

$$\hat{\rho}_B = \frac{1}{Z_{QP}} e^{-\beta(\hat{H}_{QP} - \sum_l \mu_l \hat{N}_{QP,l})}. \quad (21)$$

This choice immediately satisfies  $\mathcal{L}_B \hat{\rho}_B = 0$ . Here,  $\beta = 1/k_B T$ , with  $T$  the temperature of the superconductors, which we assume to be equal.

Let us now discuss the consequences of considering the Cooper pairs as part of the system. To begin with, the degrees of freedom for the system are now given by  $(\chi, \mathbf{M})$  [50], where  $\chi \in \{0, \uparrow, \downarrow, 2\}$  labels the quantum dot Fock states  $\{|\chi\rangle\}$ , and  $\mathbf{M} = (M_L, M_R)$  is a vector whose elements are the Cooper pair numbers of each superconductor. As a result, we can write the residue operators as [67, 72]

$$\hat{r}_S(\lambda) = \sum_{\mathbf{M}, \mathbf{m}} \hat{r}(\mathbf{m}, \mathbf{M}; \lambda) |\mathbf{M} + \mathbf{m}\rangle \langle \mathbf{M}|, \quad \lambda \in \{\lambda_i\}, \quad (22)$$

where each  $\hat{r}(\mathbf{m}, \mathbf{M}; \lambda)$  is now an operator in the QD sector only. Here,  $\mathbf{m}$  describes an imbalance in Cooper pair numbers between the bra and ket parts of the residue operator and its components can in principle take any value, positive or negative.

Let us note next that

$$i\hbar \mathcal{L}_{CP} |\mathbf{M} + \mathbf{m}\rangle \langle \mathbf{M}| = 2\mathbf{m} \cdot \boldsymbol{\mu} |\mathbf{M} + \mathbf{m}\rangle \langle \mathbf{M}|, \quad (23)$$

where we have defined a chemical potential vector  $\boldsymbol{\mu} = (\mu_L, \mu_R)$ . Due to Eq. (23), the kernels are not explicitly dependent on  $\mathbf{M}$  as only  $\mathcal{L}_{CP}$  appears in the propagators. In fact, only the Cooper pair ‘‘imbalance’’  $\mathbf{m}$  is actually relevant for the calculation of the current [72, 77]. In order to take advantage of this, let us define

$$\hat{r}(\mathbf{m}; \lambda) = \sum_{\mathbf{M}} \hat{r}(\mathbf{m}, \mathbf{M}; \lambda). \quad (24)$$

In particular,  $\hat{r}(\mathbf{0}; \lambda)$  corresponds to the partial trace over the Cooper pair sector of  $\hat{r}_S(\lambda)$ . Meanwhile, the  $\hat{r}(\mathbf{m} \neq \mathbf{0}; \lambda)$  are sums over off-diagonals in the Cooper pair sector of the full operator. Hermiticity of the system density operator requires that  $\hat{r}(\mathbf{m}; \lambda) = [\hat{r}(-\mathbf{m}; \lambda^*)]^\dagger$ . Moreover, for any matrix element  $[\hat{r}(\mathbf{m})]_{\chi'}^\chi = \langle \chi' | \hat{r}(\mathbf{m}) | \chi \rangle$ , the particle number selection rules enforce

$$N_{\chi'} - N_\chi + 2 \sum_l m_l = 0, \quad (25)$$

with  $N_\chi$  the number of particles in state  $|\chi\rangle$ . The number of particles in the SIAM is limited by the exclusion principle to be at most 2. This, together with Eq. (25), means that

$$-1 \leq m_L + m_R \leq 1. \quad (26)$$

However, there is still an infinite number of possible Cooper pair imbalances  $\mathbf{m}$  because  $m_L$  and  $m_R$  are *differences* in Cooper pair numbers and can be negative. The QD density matrix elements  $[\hat{r}(\mathbf{m})]_\chi^\chi$  with  $m_L + m_R = \pm 1$  necessarily involve coherences between the QD states with even parity (i.e.  $|0\rangle\langle 2|$  or  $|2\rangle\langle 0|$ ). Meanwhile, terms with  $m_R + m_L = 0$  entail matrix elements of  $\hat{r}(\mathbf{m})$  consistent with particle conservation (i.e. the populations and the coherences  $|\uparrow\rangle\langle\downarrow|, |\downarrow\rangle\langle\uparrow|$ ). Spin coherences can be neglected in the stationary state due to spin superselection rules [47].

The  $\hat{r}(\mathbf{m})$  can be found by directly solving the set of coupled equations [67, 72, 77]

$$(\mathcal{L}_{QD} - i\omega_{\mathbf{m}} - \lambda) \hat{r}(\mathbf{m}; \lambda) + \sum_{\mathbf{m}'} \tilde{\mathcal{K}}(\mathbf{m} - \mathbf{m}'; \lambda + i\omega_{\mathbf{m}'}) \hat{r}(\mathbf{m}'; \lambda) = 0, \quad (27)$$

where

$$\omega_{\mathbf{n}} \equiv 2\mathbf{n} \cdot \boldsymbol{\mu} / \hbar, \quad (28)$$

and

$$\tilde{\mathcal{K}}(\mathbf{m} - \mathbf{m}'; \lambda + i\omega_{\mathbf{m}'}) = \sum_{\mathbf{M}'} \langle \mathbf{M} + \mathbf{m} | [\tilde{\mathcal{K}}_S(\lambda) | \mathbf{M}' + \mathbf{m}' \rangle \langle \mathbf{M}' |] | \mathbf{M} \rangle, \quad (29)$$

is a superoperator in the QD space. It can be obtained by collecting the kernel elements which change the Cooper pair numbers by  $\mathbf{m} - \mathbf{m}'$ . The shift  $\lambda \rightarrow \lambda + i\omega_{\mathbf{m}'}$  in Eq. (27) accounts for the action of  $\mathcal{L}_{CP}$  after the CP operators in the kernel have been applied on an initial operator of the form  $|\mathbf{M}' + \mathbf{m}'\rangle \langle \mathbf{M}'|$ , as  $\lambda$  and  $\mathcal{L}_{CP}$  appear together in the propagators [see Eq. (18)]. The derivation of these expressions is given in more detail in Appendix B. In particular, see Eqs. (B5) and (B6).

### E. The ac Josephson effect

Given the equations obeyed by the residue operators, we can provide the explicit form of the frequencies  $\lambda_i$  that are relevant in the steady state. We first notice that Eq. (27) is invariant under the transformation

$$\lambda \rightarrow \lambda + i\omega_{\mathbf{n}}, \quad \mathbf{m} \rightarrow \mathbf{m} - \mathbf{n}. \quad (30)$$

Let us consider  $\lambda = 0$  first. We know that this is always a solution of the GME, and as such  $\hat{r}(\mathbf{m}; 0)$  must satisfy Eq. (27). Then, it follows from Eq. (30) that  $\hat{r}(\mathbf{m} - \mathbf{n}; i\omega_{\mathbf{n}})$  obeys the same equation. In particular,

provided that there is a single solution with  $\lambda = 0$  to Eq. (27) (which we assume in the following), we find

$$\hat{r}(\mathbf{m}; i\omega_{\mathbf{n}}) = c_{\mathbf{n}} \hat{r}(\mathbf{m} + \mathbf{n}; 0), \quad (31)$$

for some constant  $c_{\mathbf{n}}$ . Therefore,  $i\omega_{\mathbf{n}}$  must also be valid solutions of Eq. (16) for  $\mathbf{n} \in \mathbb{Z}^2$ . As a result, the stationary operator in Eq. (14) is in general time-dependent, of the form

$$\hat{\rho}_S^\infty(t) = \sum_{\mathbf{n}} \hat{r}_S(i\omega_{\mathbf{n}}) e^{i\omega_{\mathbf{n}} t}. \quad (32)$$

The coefficients  $c_{\mathbf{n}}$  can be written as

$$c_{\mathbf{n}} = \lim_{t \rightarrow \infty} C_{\mathbf{n}}(t) = \lim_{t \rightarrow \infty} \text{Tr}_S \{ (\hat{S}_L^\dagger)^{n_L} (\hat{S}_R^\dagger)^{n_R} e^{-i2\mathbf{n} \cdot \boldsymbol{\mu} t / \hbar} \hat{\rho}_S(t) \}. \quad (33)$$

They satisfy  $c_{\mathbf{n}} = c_{-\mathbf{n}}^*$ , and  $0 \leq |c_{\mathbf{n}}| \leq 1$ . The former follows from hermiticity of the solutions of the GME and the Cooper pair coherences; the latter from the triangle inequality together with the fact that the density operator is a trace one, non-negative operator. Furthermore, as the Hamiltonian respects charge conservation, for any initial state with fixed particle number, the stationary state will also respect this property [47]. As a consequence, only coefficients  $c_{\mathbf{n}}$  with  $n_L = -n_R$  can be non-zero. This property, together with the definition of the  $i\omega_{\mathbf{n}}$  [Eq. (28)], means that the stationary time evolution is periodic in the Josephson frequency

$$\Omega_J = 2eV_b / \hbar. \quad (34)$$

As a result of having a time-dependent stationary state, the ac Josephson effect follows naturally from Eq. (19). Explicitly, the current is given in the stationary state by

$$I^\infty(t) = \sum_{\mathbf{n}} I_{\mathbf{n}} e^{i\omega_{\mathbf{n}} t}, \quad (35)$$

with the amplitudes of the current harmonics being

$$I_{\mathbf{n}} = c_{\mathbf{n}} \text{Tr}_{QD} \left\{ \sum_{\mathbf{m}} \tilde{\mathcal{J}}(\mathbf{n} - \mathbf{m}; i\omega_{\mathbf{m}}) \hat{r}(\mathbf{m}; 0) \right\}. \quad (36)$$

Because the current can be written fully in terms of the operators  $\hat{r}(\mathbf{m}; 0)$ , it suffices to calculate only the  $\lambda = 0$  components. Hence, in the following we denote  $\hat{r}(\mathbf{m}; 0)$  simply by  $\hat{r}(\mathbf{m})$ . The other harmonics of the stationary state  $\hat{r}(\mathbf{m}; i\omega_{\mathbf{n}})$  can be obtained from  $\hat{r}(\mathbf{m})$  via Eq. (31).

For the mean field Hamiltonian considered here, the model lacks a dissipative or dephasing mechanism in the Cooper pair sector, due to the uncoupling between the condensate and the quasiparticle degrees of freedom, as discussed in Section II A. As a result, the coefficients  $C_{\mathbf{n}}(t)$  defined in Eq. (33) are time-independent. Then, the  $c_{\mathbf{n}}$  can be formally obtained from the initial density operator of the junction, which must be provided. This is discussed in detail in Appendix B. Nonetheless, in the

presence of a dissipation mechanism for the Cooper pair sector, the information about the initial state will be lost in the steady state and the value of the coefficients will be set dynamically by the relevant relaxation mechanism.

In the following, we consider as an ansatz coefficients of the form

$$c_{\mathbf{n}} = \delta_{n_L, -n_R} e^{i(n_R - n_L)\varphi_0/2}, \quad (37)$$

for a given phase difference  $\varphi_0$ . This choice is motivated from a reasonable initial state in Appendix B. Moreover, it reproduces the standard ‘‘BCS’’ result for the functional dependence of the supercurrent on the phase [see Eq. (43) below], allowing us to compare directly to previous results in the literature. A full description of the Cooper pair dynamics, including phase relaxation, is beyond the scope of this work.

### III. PERTURBATION THEORY

After describing the generalities of the GME and its solutions, we discuss a perturbative procedure to evaluate the density operator and the current. The following approach extends the Liouville space formulation of quantum dot transport developed recently (see e.g. [47]) to superconductivity, following similar principles to Refs. [49, 50].

The problem at hand is made particularly difficult by the combination of three factors: (1) the coupling with the leads, especially for a non zero bias voltage, (2) the Coulomb interaction in the quantum dot, and (3) the superconducting correlations at finite bias, which result in an infinite set of coupled equations for the residue operator [namely, Eq. (27)]. In order to properly account for (1) and (2), we treat the kernel perturbatively in the tunneling Hamiltonian, while keeping the interaction exactly. If we do so, (3) is also simplified considerably, since only a finite number of Cooper pairs can be transferred through the junction at any given perturbation order. As we will show in Appendix C, this means that only few terms will be relevant at any given perturbation level.

In this work, we focus on the first two non-vanishing perturbation orders in the tunneling amplitudes. As mentioned above, only even powers of  $\mathcal{L}_T$  enter the full expression of the kernel in Eq. (17). As such, it is convenient to introduce as a perturbative parameter the quantity

$$\Gamma_l = (2\pi/\hbar) G_{0,l} |t_l|^2. \quad (38)$$

Here  $G_{0,l}$  is the density of states (DOS) of lead  $l$  in the normal state, evaluated at the Fermi energy. In the following we will consider identical leads and tunneling amplitudes, so that  $\Gamma_l \equiv \Gamma$ ,  $G_{0,l} \equiv G_0$  and  $\Delta_l \equiv \Delta \in \mathbb{R}$  for  $l = L, R$ , but we will keep the label  $l$  in these quantities for the sake of generality.

The propagation and current kernels are given, to second-to-lowest order, by

$$\tilde{\mathcal{K}}_S(\lambda) = \tilde{\mathcal{K}}_S^{(1)}(\lambda) + \tilde{\mathcal{K}}_S^{(2)}(\lambda) + \mathcal{O}(\Gamma^3), \quad (39)$$

$$\tilde{\mathcal{J}}_S(\lambda) = \tilde{\mathcal{J}}_S^{(1)}(\lambda) + \tilde{\mathcal{J}}_S^{(2)}(\lambda) + \mathcal{O}(\Gamma^3), \quad (40)$$

with  $\tilde{\mathcal{K}}_S^{(k)}, \tilde{\mathcal{J}}_S^{(k)} \propto \Gamma^k$ . These correspond to the  $k = 0, 1, \dots$  terms in Eq. (17). In particular, the first order is given by

$$\tilde{\mathcal{K}}_S^{(1)}(\lambda) \bullet = \text{Tr}_{QP} \left\{ \mathcal{L}_T \tilde{\mathcal{G}}_0(\lambda) \mathcal{L}_T \bullet \otimes \hat{\rho}_B \right\}, \quad (41)$$

and the second order by

$$\tilde{\mathcal{K}}_S^{(2)}(\lambda) \bullet = \text{Tr}_{QP} \left\{ \mathcal{L}_T \tilde{\mathcal{G}}_0(\lambda) \mathcal{L}_T \mathcal{Q} \tilde{\mathcal{G}}_0(\lambda) \mathcal{Q} \mathcal{L}_T \tilde{\mathcal{G}}_0(\lambda) \mathcal{L}_T \bullet \otimes \hat{\rho}_B \right\}. \quad (42)$$

The current kernel is obtained by substituting the left-most instance of  $\mathcal{L}_T$  with the current operator  $\hat{I}$  in these expressions.

In the perturbative approach, the Josephson current appears in general as a second-order process in  $\Gamma$ , as it involves the coherent transfer of one Cooper pair (i.e. two electrons) from one superconductor to the other through the quantum dot. As such, its full description requires considering up to second order in the kernel. At the same time, the formalism presented here allows one to study arbitrary interaction strengths and gap amplitudes in an out of equilibrium situation, provided that  $\hbar\Gamma$  is the smallest energy scale in the problem. The cases of both zero and infinite gap can be recovered in the appropriate limits.

Within the perturbative expansion of Eqs. (39) and (40), we anticipate a current of the form

$$I(t) = I_0 + I_c \sin(\varphi_0 + \Omega_J t) + I_r \cos(\varphi_0 + \Omega_J t), \quad (43)$$

with the Josephson frequency  $\Omega_J$  defined in Eq. (34). The three terms in Eq. (43) derive from the truncation of the harmonic series for the current in Eq. (36) to the terms  $\mathbf{n} = \mathbf{0}$  and  $\mathbf{n} = (\pm 1, \mp 1)$ . The former yields the dc term  $I_0$ . The sum of the latter has been written as a sine term with critical current  $I_c$ , the supercurrent, and a cosine term with amplitude  $I_r$  which yields a phase-dependent dissipative current [83, 84]. Denoting it as a ‘‘dissipative current’’ is warranted in the sense that  $I_n(-V_b) = -I_n(V_b)$  for both  $n = 0, r$ , while  $I_c(-V_b) = I_c(V_b)$ . This last property ensures that there can be a non-zero current at zero bias as long as the phase difference between the two superconductors is not zero (modulo  $\pi$ ). Further harmonics will appear at higher orders in  $\Gamma$ , but we will not consider them in this work.

#### A. First order: sequential tunneling

As a first step, we keep only terms of order  $\Gamma$  in the kernels, yielding the so-called sequential tunneling approximation. The kernel, given by Eq. (41), entails two

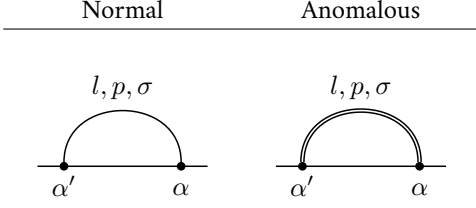


Table I. The two types of diagrams contributing to the first order kernel: (left) normal and (right) anomalous. The first one accounts for quasiparticle transport; the latter includes a Cooper pair and connects populations to Cooper pair coherences.

tunneling events, each associated with an instance of the tunneling Liouvillian  $\mathcal{L}_T$ . These events are correlated by the overall trace over the bath. In the superconducting case, the Bogoliubov-Valatin transformation, Eq. (3), allows for two distinct processes. On the one hand, the trace may be performed over two electron-like or two hole-like excitations of opposite hermiticity (see [72, 77] for details). These two contributions do not change the number of Cooper pairs. When further summing over the Cooper pairs according to the prescription in Eq. (27), these terms combine to yield the so-called *normal* kernel. It has the form

$$\tilde{\mathcal{K}}_N^{(1)}(\mathbf{0}; \lambda) = \frac{1}{i\hbar} \sum_{l,\sigma} \sum_{p,\alpha\alpha'} |t_l|^2 \alpha' \alpha \int_{-\infty}^{\infty} dE \times \mathcal{D}_\sigma^{\bar{p}\alpha'} \frac{G_{N,l}(E) f(\alpha E)}{E - i\hbar\mathcal{L}_{QD} + p\mu_l + i\hbar\lambda} \mathcal{D}_\sigma^{p\alpha}, \quad (44)$$

where  $f(E) = 1/(1 + e^{\beta E})$  is the Fermi function, accounting for the equilibrium distribution of the quasiparticles. We introduced the quantum dot superoperators  $\mathcal{D}_\sigma^{p\alpha}$ , labeled by a Liouville index  $\alpha$ , indicating that the operator acts from the left ( $\alpha = +$ ,  $\mathcal{D}_\sigma^{p+} \bullet = \hat{d}_\sigma^p \bullet$ ) or from the right ( $\alpha = -$ ,  $\mathcal{D}_\sigma^{p-} \bullet = \bullet \hat{d}_\sigma^p$ ). The Fock index  $p$  indicates hermiticity ( $p = +$ ,  $\hat{d}_\sigma^+ = \hat{d}_\sigma^\dagger$ ,  $p = -$ ,  $\hat{d}_\sigma^- = \hat{d}_\sigma$ ). The value of  $\mathcal{L}_{QD}$  in the denominator can then be determined via  $i\hbar\mathcal{L}_{QD} |\chi\rangle \langle \chi'| = (E_\chi - E_{\chi'}) |\chi\rangle \langle \chi'|$ , with  $\hat{H}_{QD} |\chi\rangle = E_\chi |\chi\rangle$ .

The kernel Eq. (44) is similar to that of a normal conductor with its density of states  $G_{0,l}$  replaced by

$$G_{N,l}(E) = G_{0,l} \text{Re} \left\{ \sqrt{\frac{E^2}{E^2 - |\Delta_l|^2}} \right\}, \quad (45)$$

reflecting the absence of quasiparticle excitations inside the superconducting gap. The current kernel  $\tilde{\mathcal{J}}_N^{(1)}(\mathbf{0}; \lambda)$  can be obtained in a similar manner by taking  $\alpha = +$  and inserting a factor  $e\ell/2$  inside the sum in Eq. (44), where  $\ell = (-1)^{\delta_{lL}}$ .

On the other hand, the trace over the quasiparticles may give a nonzero result when performed between

one electron and one hole excitation (or vice versa) of the same hermiticity, leaving one Cooper pair operator. Summing over the Cooper pairs according to Eq. (29) yields the anomalous kernel, given by

$$\tilde{\mathcal{K}}_A^{(1)}(p\mathbf{u}_l; \lambda) = \frac{1}{i\hbar} \sum_{\sigma} \sum_{\alpha'\alpha} p\alpha'\alpha\sigma |t_l|^2 \int_{-\infty}^{\infty} dE \times \mathcal{D}_\sigma^{\bar{p}\alpha'} \frac{G_{A,l}(E) f(\alpha E) \text{sgn}(E)}{E - i\hbar\mathcal{L}_{QD} - p\mu_l + i\hbar\lambda} \mathcal{D}_\sigma^{\bar{p}\alpha}, \quad (46)$$

where  $\mathbf{u}_L = (1, 0)$ ,  $\mathbf{u}_R = (0, 1)$ . Compared to the normal case, instead of the density of states as in Eq. (45), we find an anomalous density of states

$$G_{A,l}(E) = G_{0,l} \text{Re} \left\{ \sqrt{\frac{|\Delta_l|^2}{E^2 - |\Delta_l|^2}} \right\}. \quad (47)$$

The analytic form of the integrals appearing in Eqs. (44) and (46) is provided in Appendix E. The kernel  $\tilde{\mathcal{K}}_A^{(1)}(p\mathbf{u}_l; \lambda)$  generates superconducting coherences  $\hat{r}(p\mathbf{u}_l)$  when acting on the populations in  $\hat{r}(\mathbf{0})$ . Due to Eq. (25), the operator  $\hat{r}(p\mathbf{u}_l)$  can only have elements of the type  $|2\rangle \langle 0|$  and  $|0\rangle \langle 2|$  in the quantum dot sector. Note that allowing for  $\Delta_l, t_l \notin \mathbb{R}$  results in an additional phase factor  $\exp -ip(\arg \Delta_l + 2 \arg t_l)$  in Eq. (46).

The processes contributing to Eqs. (44) and (46) admit a diagrammatic representation [43, 47], as shown in Table I. The propagation from the initial state (to the right) towards the final state (to the left) is represented as a line. On this line, each fermion operator  $\mathcal{D}_\sigma^{p\alpha}$  is represented by a vertex, with an associated Liouville index  $\alpha$ . Each operator is linked via a contraction to another one, which is represented in the diagram via a *quasiparticle arc* connecting the two vertices. This contraction has associated indices  $l, p, \sigma$  and an energy  $E$ . For the first order in  $\Gamma$ , there are only two types of diagrams, normal and anomalous, represented in Table I. In the same spirit, diagrammatic representations have been provided in [50, 67] employing a Hilbert space formulation. The details of the Liouville diagrammatic rules to arbitrary order are given in Appendix D.

## B. Second order: cotunneling and pair-tunneling

The second order kernel is given in Eq. (42). It involves four tunneling events (i.e. one for each instance of  $\mathcal{L}_T$ ). Each kernel element is thus proportional to a bath correlator with four quasiparticle operators. Using Wick's theorem, this correlator can itself be written in terms of two contractions of two quasiparticle operators. There are three non-vanishing ways to contract four operators. The two that need to be considered are represented in the columns of Table II. We will refer to them as D and X diagrams, respectively. The third type of contraction, in which the leftmost and rightmost pairs

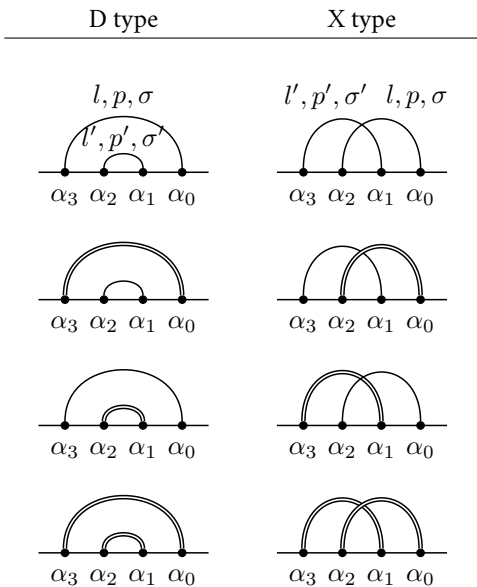


Table II. All classes of irreducible second order diagrams. Single arcs represent normal contractions while double lines represent anomalous ones. The left column displays the D type diagrams, and the right, the X type diagrams.

of vertices are contracted separately, provides a *reducible diagram*, which is canceled by the  $\mathcal{Q}$  projectors appearing in Eq. (42). In general, any diagram which can be divided into two by a vertical line without separating two vertices connected by an arc is called reducible and is canceled at this and every further perturbative level. In contrast, the D and X diagrams are *irreducible*. The differences between the D and X diagrams in a physical sense are most apparent when considering diagrammatic resummation techniques [46, 47].

In the same way as we did for the first order, we can divide the correlators according to whether the contractions are normal or anomalous. The four possible combinations correspond to the rows of Table II. In order to differentiate these terms, we write  $\tilde{\mathcal{K}}_{\psi'\psi}^{(2)}(\mathbf{m}, \lambda)$  when necessary, where  $\psi = N(A)$  if the arc associated with the rightmost vertex is normal (anomalous) and equally for  $\psi'$  for the other arc.

Kernel elements which involve two normal contractions,  $\tilde{\mathcal{K}}_{NN}^{(2)}$ , do not change the Cooper pair number and thus contribute to  $\tilde{\mathcal{K}}^{(2)}(\mathbf{0}, \lambda)$  as in the first order. Furthermore, we will have kernel elements with one normal and one anomalous arc,  $\tilde{\mathcal{K}}_{AN}^{(2)}, \tilde{\mathcal{K}}_{NA}^{(2)}$  corresponding to the diagrams represented in the second and third rows of Table II. These contribute to  $\tilde{\mathcal{K}}^{(2)}(p\mathbf{u}_l, \lambda)$  and thus act as a higher-order corrections to the anomalous terms already appearing in the sequential tunneling approximation; overall they add very little to the current almost everywhere, as can be seen from the discussion in Appendix C.

Finally, we have the kernel elements with two anoma-

lous arcs,  $\tilde{\mathcal{K}}_{AA}^{(2)}$ , corresponding to the diagrams represented in the last row of Table II. Since the quantum dot can host at most two charges, one of the arcs must create a Cooper pair, while the other must destroy one [see Eq. (26)]. These can be further separated: if the two anomalous arcs correspond to the same superconductor, the kernel contributes to  $\tilde{\mathcal{K}}^{(2)}(\mathbf{0}, \lambda)$ ; if each arc belongs to one distinct lead, the process contributes to one of

$$\tilde{\mathcal{K}}^{(2)}[(-1, 1), \lambda], \tilde{\mathcal{K}}^{(2)}[(1, -1), \lambda], \quad (48)$$

which produce the coherent transfer of one Cooper pair from one lead to the other.

#### IV. DC CURRENT

We discuss now the features appearing in the dc current  $I_0$  when out of equilibrium. Specifically, we consider  $eV_b \gg \hbar\Gamma$ . The opposite case  $eV_b \ll \hbar\Gamma$  requires retaining all the Cooper pair coherences in Eq. (27), due to the overlap of Cooper pair resonances, as discussed in Appendix C. Moreover, we consider for numerical reasons a non-zero Dynes parameter  $\zeta$  in both the normal and the anomalous density of states, corresponding to taking  $G_{l,\psi}(E) \rightarrow G_{l,\psi}(E + i\zeta)$ .

The numerical results for the differential conductance  $dI_0/dV_b$  as a function of the gate  $V_g$  and bias  $V_b$  voltages are shown in Fig. 1 (a) for the representative parameters  $U = 8$  meV,  $\Delta = 0.5$  meV,  $\hbar\Gamma = 10^{-3}$  meV. In order to understand the features seen in this figure, we distinguish between normal and anomalous (Andreev) contributions to the dc current. In particular, the dc current  $I_0$  can be written as

$$I_0 = I_{QP} + I_{\text{And}}, \quad (49)$$

where

$$I_{QP} = \text{Tr}_{QD} \left\{ \tilde{\mathcal{J}}(\mathbf{0}; 0) \hat{r}(\mathbf{0}) \right\} \quad (50)$$

is the “quasiparticle” or “normal” current, and

$$I_{\text{And}} = \text{Tr}_{QD} \left\{ \sum_{\mathbf{m} \neq \mathbf{0}} \tilde{\mathcal{J}}(-\mathbf{m}; i\omega_{\mathbf{m}}) \hat{r}(\mathbf{m}) \right\} \quad (51)$$

is the “Andreev” or “anomalous” current.

##### A. Normal current

Within the perturbative expansion considered here, the normal current can be written as

$$I_{QP} = I_{0,N} + I_{0,NN}, \quad (52)$$

where

$$I_{0,N} = \text{Tr}_{QD} \{ \tilde{\mathcal{J}}_N^{(1)}(\mathbf{0}; 0) \hat{r}(\mathbf{0}) \}, \quad (53)$$

$$I_{0,NN} = \text{Tr}_{QD} \{ \tilde{\mathcal{J}}_{NN}^{(2)}(\mathbf{0}; 0) \hat{r}(\mathbf{0}) \}. \quad (54)$$

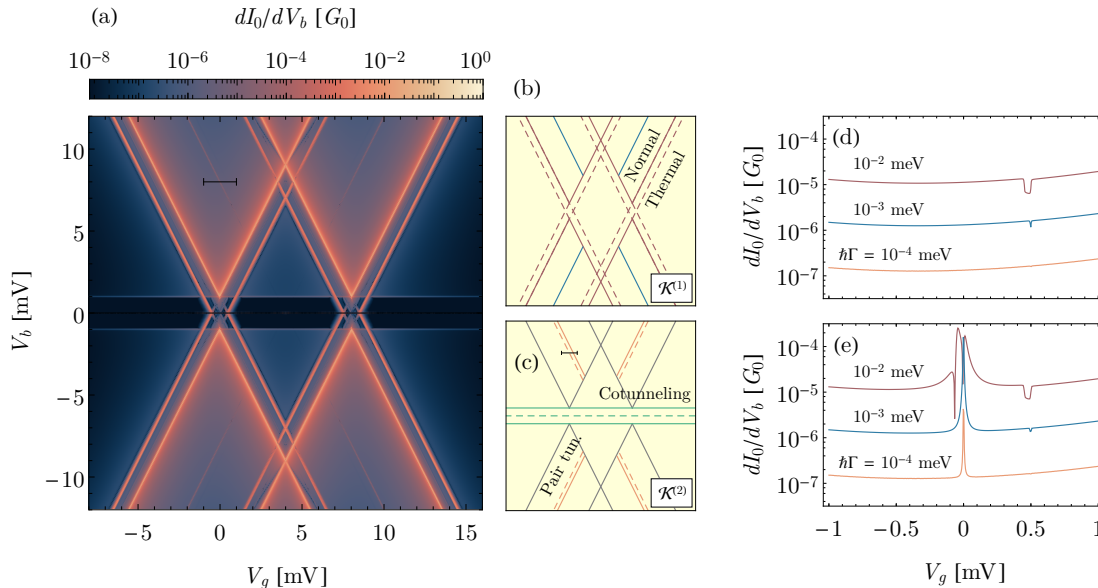


Figure 1. Differential conductance  $dI_0/dV_b$  up to the second perturbative order. (a) Stability diagram for  $dI_0/dV_b$  as a function of the gate and bias voltages,  $V_b$  and  $V_g$ , respectively. Parameters are  $\Delta = 0.5$  meV,  $U = 8$  meV,  $\hbar\Gamma = 10^{-3}$  meV,  $\zeta = 10^{-3}$  meV,  $k_B T = 0.05$  meV. A current suppression due to the quasiparticle gap is clearly observed around zero bias. (b,c) Sketch showing which features arise in first and second order, respectively. In (b) normal features from quasiparticles below the gap are represented by solid red lines, while those from thermally activated quasiparticles above the gap are represented by dashed lines. The resonance due to anomalous pair tunneling is represented in blue. In (c) we have indicated elastic cotunneling (green) and normal pair tunneling (orange) features. (d,e) Differential conductance for  $eV_b = U = 8$  meV as a function of the gate voltage without (d) and with (e) anomalous contributions and for different values of  $\hbar\Gamma$  ( $10^{-2}$  meV,  $10^{-3}$  meV, and  $10^{-4}$  meV). The range corresponding to this figure is indicated by a black segment in (a) and (c).

For these kernels, the only difference between a superconductor and a normal metal is the non-flat density of states. Apart from the changes to  $\hat{r}(\mathbf{0})$  due to the anomalous terms, this is equivalent to the so-called “semiconductor model” of the superconductor [78].

The normal terms produce a stability diagram which resembles the case of a SIAM coupled to non-superconducting electrodes, once the DOS is accounted for. In a similar way to that case, one observes areas of reduced current due to the Coulomb interaction, the well-known Coulomb diamonds, and areas of current flow, which take the form of triangles, pointing at the charge degeneracy points  $eV_g = 0, U$ . In addition, in the superconducting case, the gap opens a region of reduced current for

$$-2\Delta < eV_b < 2\Delta. \quad (55)$$

On top of that, additional resonant lines running parallel to the Coulomb diamonds and intersecting at  $V_b = 0$  can be observed. At these resonances, the current is carried by thermally excited quasiparticles above the gap, originating from the exponential tail of the Fermi function [79]. In Fig. 1 (b) we have represented schematically the main features appearing in the first order of perturbation theory, distinguishing normal contributions arising from quasiparticles below the gap (solid lines) and from the thermally excited quasiparticles (dashed lines).

Moreover, we point out the presence of a faint feature exactly at the middle point between the normal and thermal lines, which is visible especially for voltages satisfying Eq. (55). This feature is the result of a non-zero subgap density of states due to the Dynes parameter. Then,  $f(E)G_l(E)$  exhibits a small step at  $E = 0$  due to the Fermi function and, as a result, one observes a faint conductance peak.

The main processes appearing at the second order are due to long-range virtual tunneling of quasiparticles across the dot, in the form of cotunneling, and pair tunneling. These features are represented schematically in Fig. 1 (c).

Cotunneling leads to the presence of a significant current in the Coulomb diamonds, larger than the contribution from the first order term. In the case of superconducting leads, cotunneling is suppressed for the range in Eq. (55) due to the unavailability of quasiparticle excitations inside the superconducting gap. As a result, the onset of cotunneling can be appreciated as a horizontal feature [85, 86] (i.e. independent of the gate voltage  $V_g$ ) in the differential conductance at  $\pm 2\Delta/e$ , which can be seen clearly in Fig. 1 (a). It corresponds to the solid green lines in the scheme of Fig. 1 (c). Thermal effects also result in a finite current, albeit strongly reduced, extending to  $eV_b = 0$  and producing a zero-bias conductance peak [86] [represented with a dashed red line in

Fig. 1 (c)].

Quasiparticle pair tunneling involves the simultaneous transfer of two charges between the leads. Normal pair tunneling occurs prominently under the condition

$$-2eV_g + U + (-1)^{\delta_{l,L}} eV_b = 2|\Delta_l|, \quad (56)$$

which can be obtained by inspection of the integrals appearing in the pair tunneling kernel [86]. These resonances lines are displaced by a factor  $|\Delta_l|$  from the pair tunneling condition for non-superconducting leads, which corresponds to

$$-2eV_g + U + (-1)^{\delta_{l,L}} eV_b = 0. \quad (57)$$

However, thermal effects extend the area of effective pair tunneling from Eq. (56) to Eq. (57). This is indicated in the scheme of Fig. 1 (c) by orange lines (again, solid for the non-thermal and dashed for the thermal contributions).

The dc current calculated without anomalous terms is represented for a small window around the pair tunneling resonance in Fig. 1 (d), for  $eV_b = 8$  meV and different values of  $\hbar\Gamma$ . This window is marked in Fig. 1 (a) by a black segment. We observe a conductance dip corresponding to normal pair tunneling at  $eV_g = 0.5$  meV  $= \Delta$  which becomes appreciable for  $\hbar\Gamma > 10^{-3}$  meV and becomes more marked for  $\hbar\Gamma = 10^{-2}$  meV. The thermal pair tunneling feature would appear as a peak or dip for the condition in Eq. (57) for larger tunneling rates and/or temperatures, but is too faint to be seen for the parameters considered here.

## B. Andreev current

We consider now the Andreev current, corresponding to the anomalous contribution to the out of equilibrium dc current. It can be contrasted with the Josephson current, which is time-dependent for non-zero bias. In particular, the Andreev current occurs due to Cooper pair tunneling between a single superconducting lead and the quantum dot, whereas the Josephson current develops due to Cooper pair flow between two superconducting leads.

In the weak-coupling approximation, the Andreev current is given by

$$I_{\text{And}} = I_{0,A} + I_{0,AA}. \quad (58)$$

The first term originates from the first-order current kernel, and is of the form

$$I_{0,A} = \text{Tr}_{QD} \left\{ \sum_{p,l} \tilde{\mathcal{J}}_A^{(1)}(\vec{p}\mathbf{u}_l; i2p\mathbf{u}_l \cdot \boldsymbol{\mu}/\hbar) \hat{r}(p\mathbf{u}_l) \right\}. \quad (59)$$

If the lead indices in the arguments of the kernel and the coherence were not the same, this term would contribute

to the Josephson current [see also Fig. 2 (d)]. Note that, despite involving a first order kernel, these terms are  $\propto \Gamma^2$  except at the pair tunneling resonances (this is discussed in more detail in Appendix C).

The second contribution originates from the second-order anomalous kernel, and reads

$$I_{0,AA} = \text{Tr}_{QD} \{ \tilde{\mathcal{J}}_{AA}^{(2)}(\mathbf{0}; 0) \hat{r}(\mathbf{0}) \}, \quad (60)$$

where the two anomalous arcs of  $\tilde{\mathcal{J}}_{AA}^{(2)}(\mathbf{0}; 0)$  belong to the same lead. These terms are always  $\propto \Gamma^2$ .

In Fig. 2 (a), we have represented the Andreev conductance  $dI_{\text{And}}/dV_b$  for the same parameters as Fig. 1. Its main features have been schematized in Fig. 2 (b). Note that the color scale runs here from  $10^{-11}$  to  $10^{-3}$ , lowered by a factor  $\Gamma$  compared to Fig. 1 (a). Overall, the Andreev current exhibits a similar profile as the full dc current, with “normal” features along the edges of the Coulomb diamonds, indicated by solid red lines in Fig. 2 (b). These lines originate from the coherence peaks of the anomalous DOS, due to the presence of a large number of energetically available quasiparticles near the gap [72]. Moreover, we find a peak in the conductance along the thermal lines [depicted with red dashed lines in the scheme of Fig. 2 (b)] for identical reasons.

The other prominent feature is a resonant behavior along the pair tunneling condition [namely Eq. (57), marked in blue in both Fig. 1 (b) and Fig. 2 (b)]. Under resonance, the Andreev current is  $\propto \Gamma$  instead of the usual  $\propto \Gamma^2$ , despite involving the exchange of two particles. This scaling is shown rigorously in Appendix C. However, anomalous pair tunneling is significantly reduced inside the  $N = 1$  Coulomb diamond, where the Cooper pair coherences  $\hat{r}(\pm\mathbf{u}_l)$  are thermally suppressed. We have shown the Andreev current  $I_{0,A}$  along one of the two resonances in Fig. 2 (c), exhibiting both the  $\propto \Gamma$  scaling and the suppression in the first Coulomb diamond. In Fig. 1 (e) we depicted the differential conductance calculated with all of the terms in the kernel, including the anomalous contributions for the same parameters as in Fig. 1 (d). We observe a strong feature precisely at the pair tunneling resonance at  $V_g = 0$  mV, as opposed to the resonance feature due to the normal processes, which is displaced by  $\Delta$  from the resonance condition, Eq. (57).

Moreover, in the current regions outside of the Coulomb diamonds, we find a remarkable feature: a bias-independent dip in the conductance (i.e. a vertical line) for gate voltages corresponding to the degeneracy points  $eV_g = 0, U$ . This is the most distinct feature originating from  $I_{0,AA}$ , and reflects its vanishing along these lines. At  $eV_g = 0$ , we can obtain an analytic expression for  $I_{0,AA}$  in the limit  $\mu_l \ll U$ . Under this condition, the contributions to the Andreev current from both leads cancel each other due to symmetry and the equal populations of the empty and single occupied states. For  $eV_g = U$ , the same logic follows due to particle-hole symmetry of the stability diagram along the line  $eV_g = U/2$ . This is shown in more detail in Appendix G.

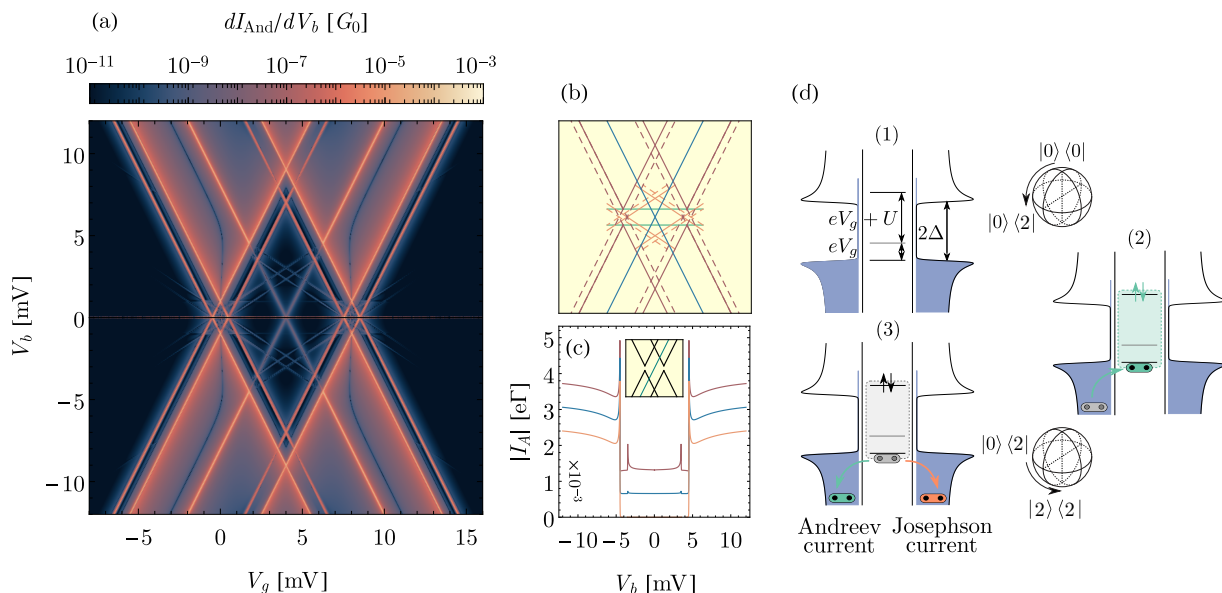


Figure 2. Andreev current and differential conductance up to the second perturbative order. (a) Stability diagram depicting  $dI_{\text{And}}/dV_b$  as a function of the gate and bias voltages,  $V_b$  and  $V_g$ , respectively. (b) Scheme with the main resonances observed in panel (a). In red: normal features (dashed lines indicate thermal processes). In blue: pair tunneling. In orange: faint low-slope features characteristic of anomalous transport. (c) Andreev current  $I_A$  along the green resonance line in the inset, for different values of  $\hbar\Gamma$  according to Eq. (57) (for  $l = L$ ). The curves for different  $\hbar\Gamma$  are displaced for visibility. (d) Scheme of the pair transfer process. From top to bottom: (1) Energetics of the junction. (2) The tunneling of a Cooper pair produces a Cooper pair coherence; in the quantum dot space, this is  $|0\rangle\langle\uparrow\downarrow|$ . (3) The Cooper pair is then transferred to another lead. If it comes back to the lead it originated from, it contributes to the dc Andreev current; on the other hand, if it tunnels to the opposite lead, it contributes to the time-dependent Josephson effect. Parameters are the same as in Fig. 1.

Finally, we have two weaker sets of peaks, corresponding to lower slope lines (compared to the Coulomb diamonds) and horizontal cotunneling-like lines. These are marked respectively by orange (solid or dashed for thermal contributions) and green lines in Fig. 2 (b). These features are visible in Fig. 2 (a) due to the lower range of the conductance, and correspond to effects which scale as  $\propto \Gamma^3$  or larger. The horizontal cotunneling-like lines (marked in green) are due to corrections to the density operator from the propagation kernel  $\tilde{\mathcal{K}}^{(2)}$ .

The lower slope lines, indicated in orange, are reminiscent of subgap features due to multiple Andreev reflections predicted in resonant tunneling junctions [87]. Here, however, due to the inclusion of Coulomb interactions, they occur within the Coulomb gap. While the slopes of the diamond amount to  $V_b = \pm 2V_g$ , the ones involving Cooper pair tunneling are given by  $V_b = \pm 2V_g/3$ . This reflects the energy  $eV_b$  needed to exchange a Cooper pair from one lead to the other. For the dc current, they appear as higher order corrections, which are not visible in the full result of Fig. 1, where cotunneling leads to an appreciable current inside the Coulomb diamond that masks these peaks. Processes involving the transfer of more Cooper pairs would yield even lower slopes:  $\pm 2/(2n+1)$ ,  $n \in \mathbb{N}$ , but are not observed in the weak coupling limit. Nonetheless, we remark that, in the calculations presented here, only a few effects of order  $\Gamma^3$  or

higher are accounted for. As a result, this discussion can only be understood qualitatively.

We further discuss the two contributions to the Andreev current  $I_{0,A}$  and  $I_{0,AA}$  separately in Appendix G. In particular, inside the Coulomb diamonds, the two contributions cancel each other as they come with similar magnitude but opposite sign.

## V. JOSEPHSON CURRENT

We move now to the time-dependent terms. Like we did with the Andreev current, we can differentiate contributions coming from the first order kernel, which have the form

$$\tilde{\mathcal{J}}_A^{(1)}(\mp \mathbf{u}_{\bar{l}}; \lambda) \hat{r}(\pm \mathbf{u}_l), \quad (61)$$

with  $\bar{l}$  denoting the opposite lead to  $l$  (for conciseness, here and onward we do not write explicitly the value of  $\lambda$  unless necessary). We denote the current originating from these terms as  $I_{c,A}$  and  $I_{r,A}$ , respectively for the critical and dissipative current. Note that, even if the current kernel is of first order, the contribution to the current will be of order  $\Gamma^2$  outside of the pair-tunneling resonances.

Moreover, we have terms coming from the second order

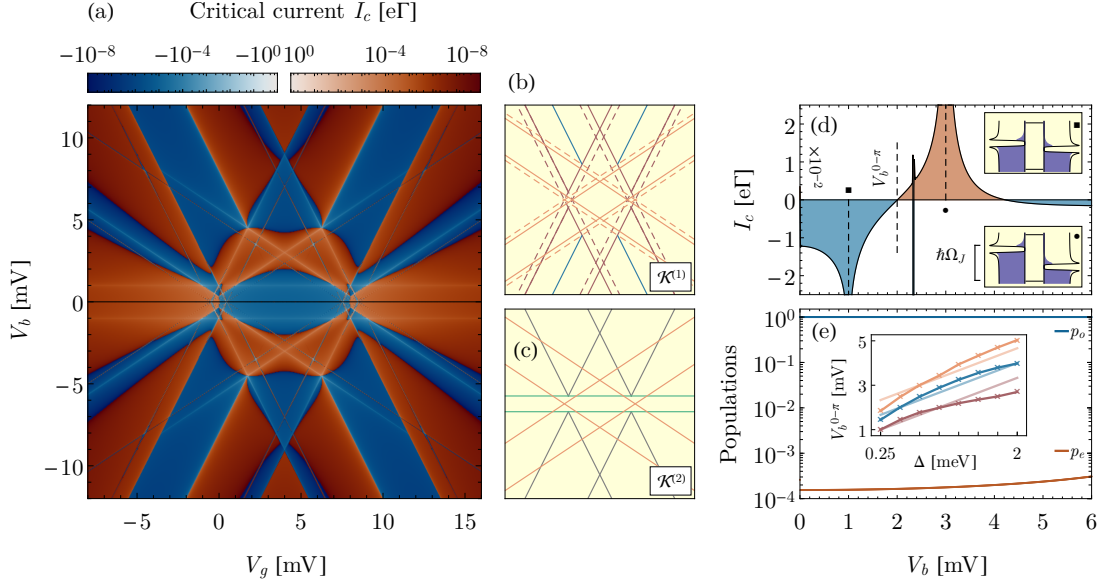


Figure 3. Critical current of the SIAM. (a) Stability diagram depicting  $I_c$  in logarithmic scale as a function of the gate and bias voltages,  $V_b$  and  $V_g$ , respectively. Noticeable is the alternance of regions with positive (red) and negative (blue) sign of the critical current. (b) The main features originating from the first order kernel. In red: lines reproducing the Coulomb diamond structure (dashed lines indicate thermal features). In blue: pair tunneling resonances due to superconducting coherences. In orange: low slope lines characteristic of anomalous transport. (c) The unique contributions due to the second order kernel. In green: cotunneling-like lines; i orange: low slope lines. (d) Critical current for  $eV_g = U/2$ . Inset: scheme of the energetics at the cotunneling-like (square) and low slope lines (dot). (e) Population of the odd (red) and even (blue) sectors. Inset: the  $0 - \pi$  transition bias as a function of the gap  $\Delta$  for  $U = 4$  (red),  $U = 8$  (blue) and  $U = 12$  (orange). The lines with lighter colors correspond to the heuristic Eq. (63). Unless noted, parameters are as in Fig. 1.

current kernel, of the form

$$\tilde{\mathcal{J}}_{AA}^{(2)}[(-1, 1); \lambda] \hat{r}(\mathbf{0}), \tilde{\mathcal{J}}_{AA}^{(2)}[(1, -1); \lambda] \hat{r}(\mathbf{0}). \quad (62)$$

We denote the resulting current terms by  $I_{c,AA}$  and  $I_{r,AA}$  for the critical and dissipative currents, respectively. The expressions for the kernels in second order are quite complex and we describe them in Appendix F. Other contributions exist, such as those coming from terms like  $\tilde{\mathcal{J}}_{NN}^{(2)}(\mathbf{0}; \lambda) \hat{r}[-1, 1]$ . Since these are of higher order in  $\Gamma$ , we do not discuss them here.

### A. Critical current

We have depicted the critical current as a function of the gate and bias voltages in Fig. 3 (a). We have represented its magnitude logarithmically as well as its sign by the color of the scale (red for positive and blue for negative sign). The features in the figure coming from the first order kernel are sketched in Fig. 3 (b), while the ones due to the second order kernel are shown in Fig. 3 (c). Moreover, the two contributions  $I_{c,A}$  and  $I_{c,AA}$  are shown separately in Fig. 4 (a) and (b). We discuss now these features.

First, the Coulomb-diamond profile can be recognized in Fig. 3 (a). Along these lines, the proximity effect is

amplified by the coherence peaks of the DOS, in a similar way to what occurs for the Andreev current. Likewise, we observe peaks in the Josephson current along the Cooper pair resonances [Eq. (57)], marked in blue in Fig. 3 (b). These peaks are due to  $I_{c,A}$ , and thus are observed in Fig. 4 (a). The proximity effect here is the largest as the unoccupied and doubly occupied states in the dot are resonant with the Cooper pairs of one of the leads, as mentioned above and discussed in detail in Appendix C. There, we show that the Josephson current along these resonances is  $\propto \Gamma$  instead of the usual  $\propto \Gamma^2$ . This is demonstrated numerically in Fig. 4 (c) and (d). In particular, (d) shows that the width of the resonance is also proportional to  $\Gamma$ . Inside the central Coulomb diamond the Cooper pair resonances are thermally suppressed and the corresponding features are no longer seen.

The characteristic feature of the critical current is the presence of low slope lines, similar to the Andreev current. These are marked in orange in Fig. 3 (b) and (c). For the Andreev current these lines correspond to higher order processes and are barely noticeable in the full dc current of Fig. 1; however, for the critical current the low slope lines are a leading order feature. Inspecting the second order kernel  $\tilde{\mathcal{J}}_{AA}^{(2)}[(-1, 1); \lambda]$ , as given in Appendix F [i.e. Eq. (F6)], one observes a characteristic factor  $3eV_b/2$  in the denominators, which results in a low slope. As mentioned in Section IV B, this reflects the en-

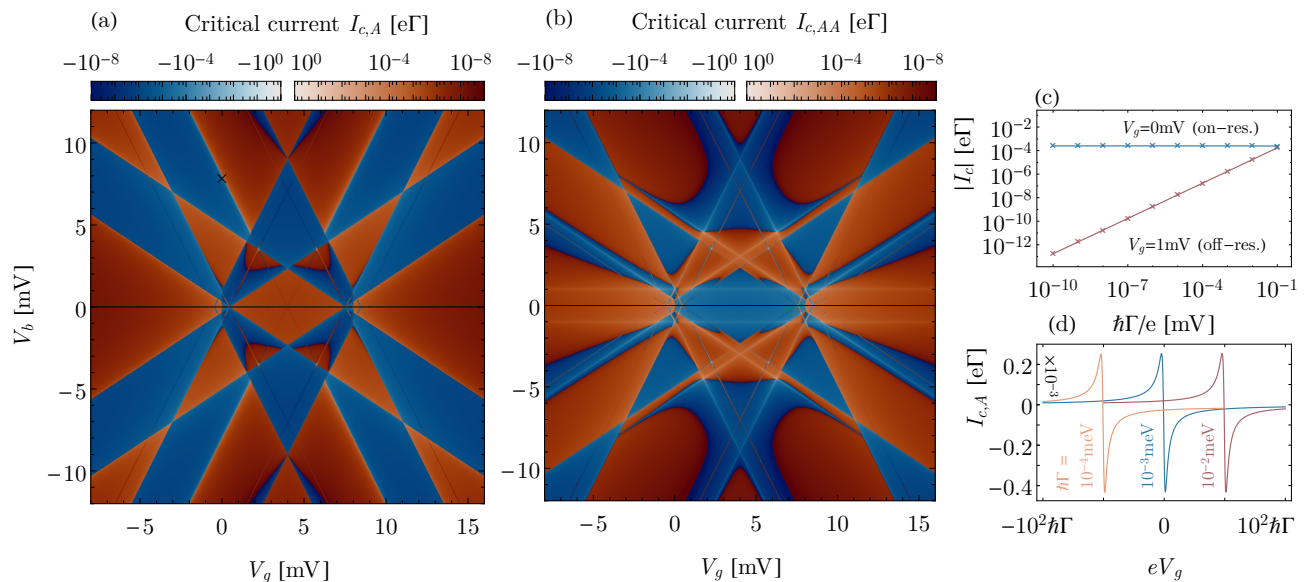


Figure 4. Contributions to the critical current originating from the first and second order current kernels. (a) Critical current  $I_{c,A}$  originating from the first order kernel, as a function of the gate and bias voltages,  $V_b$  and  $V_g$ , respectively. Parameters are the same as Fig. 1. Sign is marked by color (red for positive and blue for negative sign). (b) Same, for  $I_{c,AA}$ , arising from the second order kernel  $I_{c,AA}$ . (c) Scaling of the critical current in a Cooper pair resonance ( $V_g = 0, V_b = 8$  mV, blue) and out of resonance ( $V_g = -1$  mV,  $V_b = 8$  mV, red) for  $\hbar\Gamma = 10^{-3}$  meV. (d) The pair tunneling resonance at  $V_b = 8$  mV for  $\hbar\Gamma = 10^{-4}$ ,  $10^{-3}$ , and  $10^{-2}$  meV, displaced for clarity. The range of  $eV_g$  in the x axis has also been scaled by the value  $\hbar\Gamma$ , showing that both the current and the width of the resonance are proportional to  $\hbar\Gamma$ ,

ergy  $eV_b$  needed to exchange a Cooper pair from one lead to the other.

Finally, we observe gate-independent horizontal lines mirroring the cotunneling lines observed and discussed in the dc current. The origin of these lines is similarly the long-range transfer of charge from lead to lead with only virtual occupation of the dot. They appear only in  $I_{c,AA}$ , as can be seen in Fig. 4 (b).

The critical current exhibits a complex structure when it comes to the sign. For low bias voltages we can connect these findings to known results for the interacting SIAM at zero bias [39, 50]. We observe clearly a  $0 - \pi$  transition occurring near zero bias upon sweeping the gate voltage. It is signaled by a change of the sign of the supercurrent in the central Coulomb diamond compared to the neighboring diamonds with even occupancy. This change of sign remarkably extends to bias voltages  $|eV_b| \lesssim 3\Delta/2$ . Here, it is useful to distinguish the behavior of  $I_{c,A}$  from that of  $I_{c,AA}$ . For  $I_{c,A}$ , the critical current is mostly positive in the central Coulomb diamond, near zero bias, except for two small pockets near the degeneracy points  $eV_g = 0, U$ . Previous results in the low temperature limit  $\beta|\Delta_l| \rightarrow \infty$  indicate that the contribution from the first order kernel to the critical current is always positive [50]. However, thermal effects allow for a change of sign to occur even at this level of approximation due to quasiparticle-assisted processes. In contrast,  $I_{c,AA}$  is negative in the first Coulomb diamond for low bias, except near the resonances close to the degeneracy

points.

Inside the central Coulomb diamond, we observe another change in sign in the full critical current as the voltage bias is increased. This sign change accompanies the low slope lines at first, close to the degeneracy points. As the bias voltage is increased further, the current goes back to negative for  $eV_b \gtrsim U/2$ .

We have depicted the current for  $eV_g = U/2$  in Fig. 3 (d), as well as the populations of the odd and even sectors, namely

$$p_o = \sum_{\sigma} \langle \sigma | \hat{r}(\mathbf{0}) | \sigma \rangle,$$

$$p_e = \langle 0 | \hat{r}(\mathbf{0}) | 0 \rangle + \langle 2 | \hat{r}(\mathbf{0}) | 2 \rangle,$$

in Fig. 3 (e). Note, in particular, that the  $0 - \pi$  transition at  $eV_b = 2$  meV, seen in Fig. 3 (c), is not accompanied with a change of the parity of the ground state. Instead, we can attribute this change to the competition between two processes: the feature occurring at  $eV_b = 1$  meV (indicated with a square), with negative sign, and the one occurring at  $eV_b = 3$  meV (marked with a dot), with positive sign. The former is the gate-independent cotunneling-like feature at  $eV_b = 2\Delta$ , while the second originates from the low slope lines which meet in the center of the odd Coulomb diamond at  $eV_b = 2(U/2 + \Delta)/3$ . Here, the  $0 - \pi$  transition occurs precisely at the middle point between these two resonances. Following this logic, we can obtain a heuristic expression for the first  $0 - \pi$

transition at  $eV_g = U/2$ , which will occur for values of the bias voltage given by

$$eV_b^{0-\pi} \simeq U/6 + 4\Delta/3, \quad eV_g = U/2. \quad (63)$$

We have calculated numerically  $V_b^{0-\pi}$  for different values of  $U$  and  $\Delta$ , shown in the inset of Fig. 3 (e). The heuristic curves of Eq. (63) have been represented with lighter colors. As can be seen there, they approximate qualitatively the true transition points.

Moreover, we have sketched the energetics corresponding to the two resonances in the insets of Fig. 3 (d), showcasing the distinct physics corresponding to the two resonances. The gate-independent cotunneling-like feature occurs as the peaks of the two DOS functions align. Meanwhile, the low slope line corresponds to a Cooper pair-assisted process, where the peak of the electron (empty) part of the source DOS is separated by  $\hbar\Omega_J$  from the chemical potential of the dot at the 0-1 transition.

In a similar way, in the 0 and 2 charge Coulomb diamonds, the current around the low slope lines is of opposite sign to the rest of the diamond. Outside of the diamonds,  $I_{c,A}$  undergoes a change of sign as the pair tunneling resonances are crossed, which is not present in  $I_{c,AA}$  (having no intrinsic pair tunneling features). This change in sign can be understood from the fact that the contribution to  $I_{c,A}$  from lead  $l$  is proportional to  $\approx 2eV_g + U - 2\mu_l$  [see Eq. (C1)].

We note that, due to numerical errors, the resonance lines in the critical current usually exhibit small regions of the opposite sign, e.g. in correspondence with the normal slope thermal lines, visible in both Fig. 3 and Fig. 4. We associate these localized sign issues to convergence problems when dealing with the strongly peaked density of states. We refer to Appendix F for a more detailed discussion of the numerical implementation.

## B. Dissipative contribution

The stability diagram of the dissipative contribution  $I_r$  is presented in Fig. 5. We employ the same logarithmic scale as for  $I_c$ , with the sign indicated by the color. The features of the dissipative current are similar to those of  $I_c$ . Nonetheless, we outline some differences. First, we observe horizontal cotunneling-like features. Like for the dc current, and unlike for  $I_c$ , we observe a stark reduction in the amplitude of the current for voltages  $|eV_b| < 2\Delta$ . As for the critical and Andreev currents, we observe low slope lines, doubled as well into normal and thermal lines.

Regarding the sign of  $I_r$ , we notice a similar change of sign in the central Coulomb diamond for  $|eV_b| > 2\Delta$ . Crucially, the dissipative current is odd in the bias voltage, in a similar way to the dc current. Hence, it vanishes at zero bias, leaving only the sine term in Eq. (43). We observe sign changes occurring together with the presence of low slope lines. Here, unlike for  $I_c$ , the sign change occurs along — instead of around — the resonance. Since

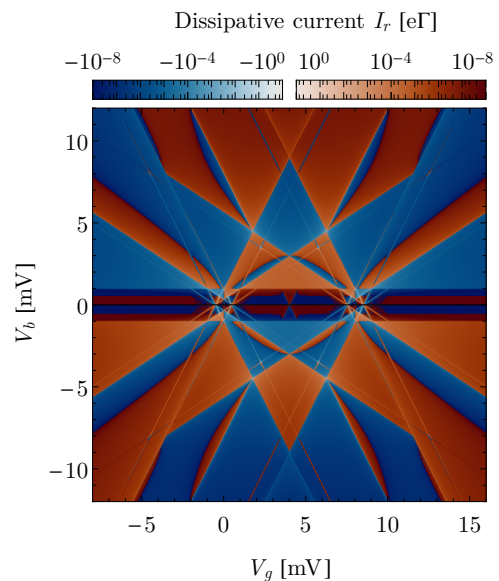


Figure 5. Dissipative contribution as a function of the gate  $V_g$  and bias  $V_b$  voltages in logarithmic scale for the same parameters as in Fig. 3. The sign of the current is color coded (red for positive sign and blue for negative sign).

$I_r$  is strongly suppressed for  $|eV_b| < 2\Delta$ , we do not expect the sign changes in this region to be remarkable.

## C. Josephson radiation

The time-dependent components of the current can be hard to detect in experimental circumstances. A viable way to do this is the measurement of the Josephson radiation [70, 75]. Hence, we close this section by considering the features that can be accessed via radiative measurements. In particular, we may consider an experimental setup similar to the one in [70]. There, a superconductor-insulator-superconductor (SIS) junction was employed as the detector, coupled to the S-QD-S junction via a waveguide resonator. The photo-assisted tunneling current through the SIS could be related to the amplitude of the Josephson current as  $I_{\text{PAT}} = C(V_b)I_J^2$ , where

$$I_J = \sqrt{I_c^2 + I_r^2}, \quad (64)$$

and  $C(V_b)$  is a voltage-dependent factor. It accounts for the current-voltage characteristic of the SIS junction and the impedance of the resonant circuit. We have shown  $I_J$  as a function of the gate and voltage bias in Fig. 6. Most of the features present in the Josephson radiation have already been discussed in Sections V A and V B. In particular, one sees both cotunneling-like features and low slope lines. The former are faint but observable in the results of [70].

## VI. CONCLUSION

In this work we have presented a full transport theory for quantum dot-based Josephson junctions. A particle-conserving theory of superconductivity in the particle number space was employed, which allows one to account for particle transfer in situations out of equilibrium. In this formulation, the Josephson effect arises naturally from the coherent dynamics of the Cooper pairs.

The theory is tailored to weakly coupled systems, whereby all processes up to second order in the hybridization strength were included. This encompasses sequential and virtual transfer of both quasiparticles and Cooper pairs. Specifically, we distinguished between the normal and the anomalous contributions to tunneling. The former conform to the usual “semiconductor model” of superconductivity [78]. The latter accounts for coherent Cooper pair transport and yields both an anomalous contribution to the dc current, the so-called Andreev current, as well as the Josephson current.

For the dc current, we have identified characteristic features at the Cooper pair-induced resonances, in which the quantum dot energetically favors the appearance of coherences involving both Cooper pairs and dot electrons. At these resonances, the current scales linearly with the tunneling rates, instead of the usual dependence on the square, and despite reflecting the transfer of two charges.

For the Josephson current, we obtained the full dependence of the critical current on the gate and on the bias voltage between the two superconducting leads. By studying its sign we have identified the extension of the well-known  $0 - \pi$  transition to out of equilibrium situations. We found, in particular, a rich behavior of the current (and its sign). While for the case of zero bias the change in sign can be related directly to the parity of the ground state, for non-zero bias these sign changes reflect a complex interplay of processes. For example, inside the Coulomb diamonds they arise from the competition between gate-independent cotunneling-like transport and Cooper-pair assisted tunneling, appearing as horizontal and low slope lines in the stability diagram, respectively. We further present results for the dissipative current and the Josephson radiation, which exhibit similar features to the critical current.

The dc current has been measured in many different setups in the past, most notably in nanowire and carbon nanotube junctions [38]. Furthermore, measuring the Josephson radiation [70, 75] allows access to information about the time-dependent quantities. From the theoretical point of view, the formalism is extremely adaptative. While we considered the particularities of a single quantum dot junction, the model can be extended to arbitrary interacting nanojunctions directly.

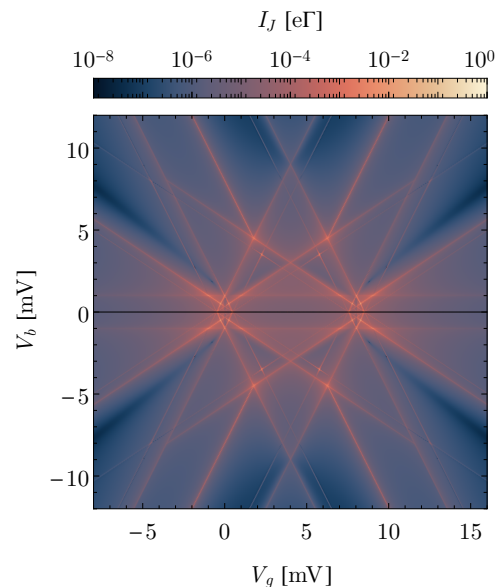


Figure 6. Josephson radiation amplitude  $I_J$  as a function of the gate and bias voltages in logarithmic scale for the same parameters as in Fig. 3.

## ACKNOWLEDGMENTS

We thank Julian Siegl for discussion and help on this work, and Christoph Brückner for help with the numerical simulations. J.P.-C. and M.G. acknowledge DFG funding through Project B04 and A.D. through Project B02 of SFB 1277 Emerging Relativistic Phenomena in Condensed Matter. G. P. is supported by Spain’s MINECO through Grant No. PID2020-117787GB-I00 and by CSIC Research Platform PTI-001.

### Appendix A: Stationary solutions of the GME

We sketch the derivation of the GME, Eq. (12), within the Nakajima-Zwanzig formalism [80, 81], focusing on the time-dependent solutions.

The full density operator, including quantum dot and leads, is a solution of the Liouville-von Neumann equation

$$\partial_t \hat{\rho}(t) = -\frac{i}{\hbar} [\hat{H}, \hat{\rho}(t)] = \mathcal{L} \hat{\rho}(t), \quad (\text{A1})$$

The Nakajima-Zwanzig projector is now introduced

$$\mathcal{P} \bullet = \text{Tr}_B \{ \bullet \} \otimes \hat{\rho}_B = (1 - \mathcal{Q}) \bullet, \quad (\text{A2})$$

with an, in principle, arbitrary reference density operator  $\hat{\rho}_B$ . Provided that  $\mathcal{L}_B \hat{\rho}_B = 0$ , we can write Eq. (A1) as an equation only for  $\mathcal{P} \hat{\rho}(t)$  as

$$\begin{aligned} \partial_t \mathcal{P}\hat{\rho}(t) &= \mathcal{P}\mathcal{L}_T \tilde{\mathcal{G}}_{\mathcal{Q}}(t) \mathcal{Q}\hat{\rho}(0) \\ &+ \mathcal{L}_S \mathcal{P}\hat{\rho}(t) + \int_0^t ds \mathcal{K}_{\mathcal{P}}(t-s) \mathcal{P}\hat{\rho}(s), \end{aligned} \quad (\text{A3})$$

[compare Eq. (12)] where we have defined

$$\mathcal{K}_{\mathcal{P}}(t-s) = \mathcal{P}\mathcal{L}_T \tilde{\mathcal{G}}_{\mathcal{Q}}(t-s) \mathcal{L}_T \mathcal{P}, \quad (\text{A4})$$

$$\tilde{\mathcal{G}}_{\mathcal{Q}}(t-s) = \exp(\mathcal{L}_S + \mathcal{L}_B + \mathcal{Q}\mathcal{L}_T \mathcal{Q})(t-s). \quad (\text{A5})$$

We moreover assume that  $\mathcal{Q}\hat{\rho}(0) = 0$ , allowing us to neglect the first term in the right-hand side of Eq. (A3).

For the time-independent case considered here, we proceed by Laplace transforming Eq. (A3), yielding

$$\begin{aligned} (\lambda - \mathcal{L}_S) \text{L}\{\mathcal{P}\hat{\rho}\}(\lambda) - \mathcal{P}\hat{\rho}(0^+) \\ = \text{L}\{\mathcal{K}_{\mathcal{P}}\}(\lambda) \text{L}\{\mathcal{P}\hat{\rho}\}(\lambda), \end{aligned} \quad (\text{A6})$$

with  $\text{L}\{f\}(\lambda) = \int_0^\infty dt e^{-\lambda t} f(t)$  denoting Laplace transformation. The time-domain solution can be recovered through Mellin's inverse formula

$$\mathcal{P}\hat{\rho}(t) = \frac{1}{2\pi i} \int_{\gamma-i\infty}^{\gamma+i\infty} d\lambda e^{\lambda t} \text{L}\{\mathcal{P}\hat{\rho}\}(\lambda), \quad (\text{A7})$$

where  $\gamma$  is a real number such that all poles of  $\text{L}\{\mathcal{P}\hat{\rho}\}(\lambda)$  lie to the left of the  $\text{Re}\{\lambda\} = \gamma$  line in the complex plane. This integral can be calculated with the use of the residue theorem, employing a semicircular contour in the left complex half-plane. Then, provided that there are only first order poles in the contour, we recover directly the time evolution

$$\mathcal{P}\hat{\rho}(t) = \sum_{\lambda_i} e^{\lambda_i t} \hat{r}_S(\lambda_i) \otimes \hat{\rho}_B, \quad (\text{A8})$$

where  $\hat{r}_S(\lambda_i)$ , defined in Eq. (15), are the residues at the poles  $\lambda_i$ . Upon taking the trace over the bath, we can define the kernel

$$\tilde{\mathcal{K}}_S(\lambda) \bullet = \text{Tr}_B\{\mathcal{L}_T \text{L}\{\tilde{\mathcal{G}}_{\mathcal{Q}}\}(\lambda) \mathcal{L}_T \bullet \otimes \hat{\rho}_B\}, \quad (\text{A9})$$

which has the expanded form of Eq. (17). Then, Eq. (A6) can be written as

$$(\lambda - \mathcal{L}_S) \hat{r}_S(\lambda_i) - \text{Tr}_B\{\mathcal{P}\hat{\rho}(0^+)\} = \tilde{\mathcal{K}}_S(\lambda) \hat{r}_S(\lambda_i), \quad (\text{A10})$$

The poles  $\lambda_i$  can be calculated by taking the limit  $\lambda \rightarrow \lambda_i$  in Eq. (A10), yielding

$$[\mathcal{L}_S - \lambda_i + \tilde{\mathcal{K}}_S(\lambda_i)] \hat{r}_S(\lambda_i) = 0. \quad (\text{A11})$$

The  $\lambda_i$  are the solutions to the non-linear eigenvalue equation

$$\det\{\mathcal{L}_S - \lambda + \tilde{\mathcal{K}}_S(\lambda)\} = 0, \quad (\text{A12})$$

Here the determinant is understood to be of the linear application  $\mathcal{L}_S - \lambda + \tilde{\mathcal{K}}_S(\lambda)$  acting on the space of operators.

Likewise, the Laplace transform of the current

$$I(\lambda) = \text{Tr}\{\text{L}\{\mathcal{J}\}(\lambda) \text{L}\{\mathcal{P}\hat{\rho}\}(\lambda)\}, \quad (\text{A13})$$

can be transformed back to real time using Mellin's inverse formula, yielding Eq. (19), with the current kernel defined in analogy to Eq. (A9), namely

$$\tilde{\mathcal{J}}_S(\lambda) \bullet = \text{Tr}_B\{\hat{I} \text{L}\{\tilde{\mathcal{G}}_{\mathcal{Q}}\}(\lambda) \mathcal{L}_T \bullet \otimes \hat{\rho}_B\}, \quad (\text{A14})$$

where  $\hat{I}$  is defined above Eq. (13).

## Appendix B: GME for the quantum dot and Cooper pairs

We particularize the Nakajima-Zwanzig formalism to the case of a central system comprising both the quantum dot states and the Cooper pairs of the leads. The action of the current kernel can be written in the following manner, separating explicitly the action on the QD and CP sectors

$$\begin{aligned} \tilde{\mathcal{J}}_S(\lambda) \hat{r}_S(\lambda) &= \sum_{\delta \mathbf{M}} \sum_{\Delta \mathbf{M}} \sum_{\mathbf{m}} \sum_{\mathbf{M}} \left( \hat{S}_L^\dagger \right)^{\delta M_L} \left( \hat{S}_R^\dagger \right)^{\delta M_R} |\mathbf{M} + \mathbf{m}\rangle \langle \mathbf{M}| \left( \hat{S}_R^\dagger \right)^{\Delta M_R} \left( \hat{S}_L^\dagger \right)^{\Delta M_L} \\ &\times \tilde{\mathcal{J}}(\delta \mathbf{M}, \Delta \mathbf{M}; \lambda + i\omega_{\mathbf{m}}) \hat{r}(\mathbf{m}, \mathbf{M}; \lambda), \end{aligned} \quad (\text{B1})$$

where  $(\hat{S}_l^\dagger)^{-m}$  is  $(\hat{S}_l)^m$ ,  $\omega_{\mathbf{m}}$  is defined in Eq. (28), and we introduce two difference vectors  $\delta \mathbf{M}$  and  $\Delta \mathbf{M}$ .

Here,  $\tilde{\mathcal{J}}(\delta \mathbf{M}, \Delta \mathbf{M}; \lambda)$  is a superoperator in the quantum dot space only. In order to arrive to an expression for it, we have to evaluate the effect of the kernel  $\tilde{\mathcal{J}}_S(\lambda)$  on

the Cooper pair sector. This action comes in two forms. First, through the presence of the Cooper pair operators, and second through the action of  $\mathcal{L}_{CP}$ , present in the free

propagators [see Eq. (18)], which needs to be resolved. In order to do so, we make use of  $i\hbar\mathcal{L}_{CP}\hat{S}_i^p = 2p\mu_i\hat{S}_i^p$ , to move the Cooper pair operators to the left, as in Eq. (B1). By this, we have included a shift  $i2\mathbf{m} \cdot \boldsymbol{\mu}/\hbar$  in the argument of the kernel in Laplace space. This accounts for

the action of  $\mathcal{L}_{CP}$  when applied to a term  $|\mathbf{M} + \mathbf{m}\rangle \langle \mathbf{M}|$  such as the one appearing in Eq. (B1). We could incorporate this as a shift in the Laplace variable  $\lambda$  because  $\lambda$  and  $\mathcal{L}_{CP}$  always appear together in the propagators.

The current can be written in terms of the  $\tilde{\mathcal{J}}(\delta\mathbf{M}, \Delta\mathbf{M}; \lambda)$  of Eq. (B1) as

$$I^{(\lambda)} = \text{Tr}_{QD} \left\{ \sum_{\Delta\mathbf{M}} \sum_{\mathbf{m}} \sum_{\mathbf{M}} \tilde{\mathcal{J}}(-\mathbf{m} - \Delta\mathbf{M}, \Delta\mathbf{M}; \lambda + i\omega_{\mathbf{m}}) \hat{r}(\mathbf{m}, \mathbf{M}; \lambda) \right\}. \quad (\text{B2})$$

Since the kernel term is independent of the index  $\mathbf{M}$ , we can move the summation over  $\mathbf{M}$  to the density operator and introduce the simplified notation

$$I^{(\lambda)} = \text{Tr}_{QD} \left\{ \sum_{\mathbf{m}} \tilde{\mathcal{J}}(-\mathbf{m}; \lambda + i\omega_{\mathbf{m}}) \hat{r}(\mathbf{m}; \lambda) \right\}, \quad (\text{B3})$$

with  $\hat{r}(\mathbf{m}; \lambda)$  defined in Eq. (24) and

$$\tilde{\mathcal{J}}(\Delta\mathbf{m}; \lambda) = \sum_{\Delta\mathbf{M}} \tilde{\mathcal{J}}(\Delta\mathbf{m} - \Delta\mathbf{M}, \Delta\mathbf{M}; \lambda). \quad (\text{B4})$$

Note that we do not denote the  $\tilde{\mathcal{J}}(\Delta\mathbf{m}; \lambda)$  in a particular manner, and distinguish them from the  $\tilde{\mathcal{J}}(\delta\mathbf{M}, \Delta\mathbf{M}; \lambda)$  by the number of arguments. This shows that only the  $\hat{r}(\mathbf{m}; \lambda)$  are needed in order to calculate the current. That is, we can freely sum over the  $\mathbf{M}$  and consider only the Cooper pair imbalance  $\mathbf{m}$ , with the information of the CP sector fully encoded into the  $\mathbf{m}$ .

We can perform a similar simplification of the GME. With Cooper pair numbers explicitly written, the equation for a term such as  $\hat{r}(\mathbf{m}, \mathbf{M}; \lambda)$  is given by

$$0 = (\mathcal{L}_{QD} + \lambda - i\omega_{\mathbf{m}}) \hat{r}(\mathbf{m}, \mathbf{M}; \lambda) + \sum_{\delta\mathbf{M}} \sum_{\Delta\mathbf{M}} \sum_{\mathbf{m}'} \sum_{\mathbf{M}'} \langle \mathbf{M} + \mathbf{m} | \left( \hat{S}_L^\dagger \right)^{\delta M_L} \left( \hat{S}_R^\dagger \right)^{\delta M_R} | \mathbf{M}' + \mathbf{m}' \rangle \\ \times \langle \mathbf{M}' | \left( \hat{S}_R^\dagger \right)^{\Delta M_R} \left( \hat{S}_L^\dagger \right)^{\Delta M_L} | \mathbf{M} \rangle \tilde{\mathcal{K}}(\delta\mathbf{M}, \Delta\mathbf{M}; \lambda + i\omega_{\mathbf{m}'}) \hat{r}(\mathbf{m}', \mathbf{M}'; \lambda), \quad (\text{B5})$$

where again we have moved the Cooper pairs to the left and evaluated the  $\mathcal{L}_{CP}$  in the same manner as for the current kernel. Then, we can sum over  $\mathbf{M}$  in Eq. (B5). Defining

$$\tilde{\mathcal{K}}(\Delta\mathbf{m}, \lambda) = \sum_{\Delta\mathbf{M}} \tilde{\mathcal{K}}(\Delta\mathbf{m} - \Delta\mathbf{M}, \Delta\mathbf{M}; \lambda), \quad (\text{B6})$$

we obtain the GME as in Eq. (27). With  $\Delta\mathbf{m} = \mathbf{m} - \mathbf{m}'$  and  $\Delta\mathbf{M} = \mathbf{M}' - \mathbf{M}$ , we see that Eq. (B6) is equivalent to Eq. (29). In this simplified notation, the term  $\tilde{\mathcal{K}}(\Delta\mathbf{m}; \lambda)$  includes all kernel elements that change the number of Cooper pairs by  $\Delta\mathbf{m}$ , regardless of whether the Cooper pair operators act on the right or on the left. This can be seen from the fact that, in Eq. (B5),  $\mathbf{m} - \mathbf{m}' = \delta\mathbf{M} + \Delta\mathbf{M}$ .

From this, the proof of Eq. (31) is direct. We can consider the NZE for a reduced quantum dot operator

$$\hat{r}(\mathbf{m}; i\omega_{\mathbf{n}})$$

$$[\mathcal{L}_{QD} - i\omega_{\mathbf{m}+\mathbf{n}}] \hat{r}(\mathbf{m}; i\omega_{\mathbf{n}}) \\ + \sum_{\mathbf{m}'} \tilde{\mathcal{K}}(\mathbf{m} - \mathbf{m}', i\omega_{\mathbf{m}'+\mathbf{n}}) \hat{r}(\mathbf{m}'; i\omega_{\mathbf{n}}) = 0.$$

This is the same equation as the one for  $\hat{r}(\mathbf{m} + \mathbf{n}; 0)$ , yielding the desired equivalence. Note that this must be satisfied for all  $\mathbf{m}$ , and hence the coefficients relating the two quantities, namely the  $c_{\mathbf{n}}$ , appearing in Eq. (31), must be independent of  $\mathbf{m}$ .

Within the mean field approximation of our model, these  $c_{\mathbf{n}}$  can be determined by considering the constant of motion

$$\text{Tr}\{(\hat{S}_L^\dagger)^{n_L} (\hat{S}_R^\dagger)^{n_R} e^{-i2\mathbf{n} \cdot \boldsymbol{\mu} t / \hbar} \hat{\rho}(t)\}. \quad (\text{B7})$$

The fact that this quantity is conserved follows from the fact that the Cooper pair operators commute with the tunneling Hamiltonian. The time-dependent factor compensates for the time evolution of the Cooper pair operators due to the chemical potential of the leads. Since

$(\hat{S}_L^\dagger)^{n_L}(\hat{S}_R^\dagger)^{n_R}$  is purely a system operator, its expectation value can be evaluated from the reduced density operator, yielding at the initial time

$$\text{Tr}_S\{(\hat{S}_L^\dagger)^{n_L}(\hat{S}_R^\dagger)^{n_R}\hat{\rho}_S(0)\}.$$

This is to be compared with its value in a stationary state given by Eq. (32),

$$\begin{aligned} & \text{Tr}_S\{(\hat{S}_L^\dagger)^{n_L}(\hat{S}_R^\dagger)^{n_R}\sum_{\mathbf{n}'}e^{i2(\mathbf{n}'-\mathbf{n})\cdot\boldsymbol{\mu}t/\hbar}\hat{r}_S(i\omega_{\mathbf{n}'})\} \\ &= \text{Tr}_{QD}\{\sum_{\mathbf{n}'}e^{i2(\mathbf{n}'-\mathbf{n})\cdot\boldsymbol{\mu}t/\hbar}\hat{r}(-\mathbf{n};i\omega_{\mathbf{n}'})\}. \end{aligned}$$

Since  $\text{Tr}_S\{\hat{r}_S(\lambda)\} = \delta_{\lambda,0}$  due to conservation of probability, together with Eq. (31), we see that  $\mathbf{n} = \mathbf{n}'$  is the only non-vanishing contribution. Then, employing this relation again

$$\text{Tr}_{QD}\{\hat{r}(-\mathbf{n};i\omega_{\mathbf{n}})\} = c_{\mathbf{n}}\text{Tr}_{QD}\{\hat{r}(\mathbf{0};0)\} = c_{\mathbf{n}},$$

and comparing this with the initial value, it follows that

$$c_{\mathbf{n}} = C_{\mathbf{n}}(0) = \text{Tr}_S\{(\hat{S}_L^\dagger)^{n_L}(\hat{S}_R^\dagger)^{n_R}\hat{\rho}_S(0)\}. \quad (\text{B8})$$

These coefficients can be related to the Fourier components of the  $F(\boldsymbol{\varphi})$  function of [72]. Here, as mentioned in the main text, we assume that Eq. (27) has a single solution for  $\lambda = 0$ . Otherwise, the different solutions to the GME may not be proportional.

Let us consider several instances of initial correlations and their corresponding  $c_{\mathbf{n}}$ . First, let us take an initial condition with no superconducting correlations, so that

$$\hat{\rho}_S(0) = \hat{\rho}_{QD}(0) \otimes \sum_{\mathbf{M}} p_{\mathbf{M}} |\mathbf{M}\rangle \langle \mathbf{M}|, \quad (\text{B9})$$

for some  $\hat{\rho}_{QD}(0)$ , with statistical weights  $p_{\mathbf{M}} \geq 0$  such that  $\sum_{\mathbf{M}} p_{\mathbf{M}} = 1$ . The  $p_{\mathbf{M}}$  reflect lack of knowledge over the total number of particles in the system. In physical terms, a state such as this arises if one considers that the leads are unconnected at  $t = 0$ , and the tunneling is switched on adiabatically afterwards, as is usual in the standard Nakajima-Zwanzig formulation. Then, it follows that  $c_{\mathbf{n}} = \delta_{\mathbf{n},\mathbf{0}}$ . Taking into account Eq. (36), we find as a result  $I^\infty(t) = I_0$  and no Josephson effect will develop in the system.

Next, we consider an initial state with a well defined phase difference between the two leads, but which still satisfies particle conservation. To do so, let us introduce the following state in the CP sector

$$|M, \varphi_0\rangle = \frac{1}{\sqrt{M+1}} \sum_{m=0}^M e^{im\varphi_0} |(M-m, m)\rangle, \quad (\text{B10})$$

which has a well-defined total particle number  $M = M_L + M_R$  but allows for a coherent superposition between states with a different distribution of Cooper pairs

between the two leads. We generalize this by taking the mixed state

$$\begin{aligned} \hat{\rho}_S(0) &= \hat{\rho}_{QD}(0) \otimes \sum_{M=0}^{\infty} p_M |M, \varphi_0\rangle \langle M, \varphi_0| \quad (\text{B11}) \\ &= \hat{\rho}_{QD}(0) \otimes \sum_{M=0}^{\infty} \sum_{m,m'=0}^M \frac{p_M}{M+1} \\ &\quad \times e^{i(m-m')\varphi_0} |(M-m, m)\rangle \langle (M-m', m')|, \end{aligned}$$

with  $\sum_M p_M = 1$ . For  $p_M \geq 0$ , this corresponds to a positive semi-definite operator which is moreover Hermitian. Note that averaging over  $\varphi_0$  in Eq. (B11) would yield a state of the form of Eq. (B9). The coefficients for this initial state are given by

$$\begin{aligned} c_{\mathbf{n}} &= \delta_{n_L, -n_R} e^{i(n_R - n_L)\varphi_0/2} \\ &\quad \times \sum_{M=\max\{0, n_L\}}^{\infty} p_M \frac{M+1 - |n_L|}{M+1}. \quad (\text{B12}) \end{aligned}$$

If the statistical weights  $p_M$  are centered around a value of  $M$  that is much larger than  $|n_L|$ , the sum is approximately equal to 1, yielding Eq. (37). This choice allows us to properly account for relaxation processes in the absence of a dc-bias, which would bring the phase to the minimum  $\varphi_0$  of the Josephson potential  $V(\varphi)$  [78].

### Appendix C: Analysis of the Cooper pair space structure

A complication with calculating the current within the theory outlined above is that the residue operator is infinitely sized, as it incorporates coherences with infinitely many Cooper pair numbers. However, not all of these elements contribute in the same manner to the current. Coherences involving large imbalances in the Cooper pair numbers between the two leads can only be produced by high order tunneling events. Hence, in the weak coupling approximation employed here we expect that they will be negligible. As such, we have not only to consider which kernel elements are relevant (as was done above) but also which residue operator coherences are. In this appendix, we develop the recipe for determining which coherences are relevant at a given perturbation level.

#### 1. Relevant contributions to the residue operator

Let us consider first  $\hat{r}(\mathbf{0})$ . Probability conservation requires that  $\text{Tr}_{QD}\{\hat{r}(\mathbf{0})\} = 1$ , therefore the leading term in  $\hat{r}(\mathbf{0})$  will be of order  $\Gamma^0 = 1$ .

On the other hand, for a term  $\hat{r}(\mathbf{m})$  with  $\mathbf{m} \neq \mathbf{0}$ , there is no equivalent trace condition. Eq. (16) gives

$$\hat{r}(\mathbf{m}) = \frac{-1}{\mathcal{L}_{QD} - 2i\mathbf{m} \cdot \boldsymbol{\mu}/\hbar + \tilde{\mathcal{K}}(\mathbf{0}; i2\mathbf{m} \cdot \boldsymbol{\mu}/\hbar)} \times \sum_{\mathbf{m}' \neq \mathbf{m}} \tilde{\mathcal{K}}(\mathbf{m} - \mathbf{m}'; i2\mathbf{m}' \cdot \boldsymbol{\mu}/\hbar) \hat{r}(\mathbf{m}'). \quad (\text{C1})$$

Hence, in order to obtain the leading order contribution to them we need to inspect Eq. (C1) and analyze the relevant kernels at each order.

We consider at first only the sequential tunneling approximation and disregard the denominator in Eq. (C1). We know that  $\hat{r}(\mathbf{0})$  is of order 1. Hence, terms such as  $\tilde{\mathcal{K}}_A^{(1)}(\pm\mathbf{u}_l; \lambda) \hat{r}(\mathbf{0})$  will be of order  $\Gamma$ , since  $\tilde{\mathcal{K}}_A^{(1)}(\pm\mathbf{u}_l; \lambda)$  is of order  $\Gamma$ . This term appears in the sum for  $\hat{r}(\pm\mathbf{u}_l)$ , which will then be of order  $\Gamma$  itself. Higher coherences are not directly connected to  $\hat{r}(\mathbf{0})$ . For instance,  $\hat{r}[(-1, 1)]$  is connected via  $\tilde{\mathcal{K}}_A^{(1)}[(1, 0); \lambda]$  to  $\hat{r}[(0, 1)]$ , and this is connected to  $\hat{r}(\mathbf{0})$  via  $\tilde{\mathcal{K}}_A^{(1)}[(0, -1); \lambda]$ . Hence,  $\hat{r}[(-1, 1)]$  will be at least of order  $\Gamma^2$ . This indicates that the coherences in the residue operator can be ordered in a *hierarchy*, in which terms which are directly connected to  $\hat{r}(\mathbf{0})$  will be of order  $\Gamma$ , and any successive step away will be one order higher in  $\Gamma$ .

This picture changes significantly when the denominator is taken into account. The same hierarchy holds in general, but whenever a matrix element  $[\hat{r}(\mathbf{m})]_{\chi\chi'}^X = \langle \chi | \hat{r}(\mathbf{m}) | \chi' \rangle$  satisfies

$$|E_\chi - E_{\chi'} - 2\mathbf{m} \cdot \boldsymbol{\mu}| \simeq \hbar\Gamma, \quad (\text{C2})$$

the denominator is of order  $\Gamma$  itself and this component and all of the following components connected to it “skip” an order in this hierarchy. We say then that the coherence is resonant. E.g. the  $\hat{r}(\pm\mathbf{u}_l)$  are of order 1 at the resonances of Eq. (57).

For the sequential tunneling approximation, provided that the condition Eq. (C2) is satisfied by at most one value of  $\mathbf{m}$  (that is, there is no overlap between two or more resonances) only  $\hat{r}(\mathbf{0})$ ,  $\hat{r}(\pm\mathbf{u}_l)$ ,  $\hat{r}[(-1, 1)]$  are relevant for the calculation of the residue operator. Moreover,  $\hat{r}[(-1, 1)]$  is only significant wherever the  $\hat{r}(\pm\mathbf{u}_l)$  are resonant.

Regarding the second order, the main change in the structure of the kernel is that now there are also kernel components of the form  $\tilde{\mathcal{K}}_{AA}^{(2)}[(-1, 1); \lambda]$ ,  $\tilde{\mathcal{K}}_{AA}^{(2)}[(1, -1); \lambda]$ , and terms such as  $\hat{r}[(-1, 1)]$  are now directly coupled to  $\hat{r}(\mathbf{0})$ . However, they do so through a kernel component of order  $\Gamma^2$  and the hierarchy still holds. The diagrams involving one normal and one anomalous arc are similar to the  $\tilde{\mathcal{K}}_A^{(1)}(\pm\mathbf{u}_l; \lambda)$  in sequential tunneling but are one order higher in  $\Gamma$ . As a result, they are only relevant at resonances such as Eq. (57) where they give contributions of order  $\Gamma^2$  to the residue operator.

Hence, at second order it suffices to consider terms up to  $\hat{r}[(\pm 1, \mp 1) \pm \mathbf{u}_l]$  to obtain the residue operator at order  $\Gamma^2$ , provided again that there are no overlapping

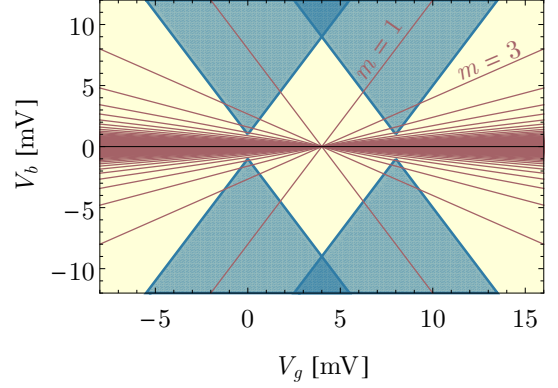


Figure 7. Cooper pair resonances in the stability diagram for  $U = 8, \Delta = 0.5$ . Red lines: Cooper pair resonances of increasingly higher order, corresponding to the condition  $2eV_g \pm mV_b + U = 0$ .

resonances. Moreover, the  $\hat{r}[(\pm 1, \mp 1) \pm \mathbf{u}_l]$  are only significant at the pair tunneling resonances.

Continuing the logic for higher orders, we can classify the possible resonances into the two types discussed under Eq. (26). First, for  $\mathbf{m} = (-m, m) \pm \mathbf{u}_l$ , with  $m \in \mathbb{Z}$ , resonances occur at

$$-2eV_g + U \pm mV_b = 0, \quad (\text{C3})$$

These are resonant along lines with progressively lower slopes  $2/m$  in the stability diagram, until eventually accumulating near  $V_b = 0$  for large  $m$ . This is shown in Fig. 7.

Second, for  $\mathbf{m} = (-m, m)$ , all of the coherences are resonant only for  $V_b = 0$ , regardless of  $m$ . As such, considering only the coherences up to a certain  $m$  in the residue operator is justified when sufficiently far ( $\sim \Gamma^k$ ) from zero bias. A resummation can nonetheless be carried out for  $V_b = 0$  exactly [50]. The collapse of the hierarchy at zero bias reflects the degeneracy of the different Cooper pair number states in that case, since there is no energy transfer from one lead to the other when a Cooper pair is exchanged.

From this, we see that the overlap of resonances in the weak coupling limit occurs only close to  $V_b = 0$ .

## 2. Relevant contributions to the current

We turn now to the current. Therefore, we apply the current kernel superoperator to the residue operator and inspect the scaling with  $\Gamma$ .

For the sequential tunneling approximation, if no resonances are present, the main contribution to the dc current will come from  $\tilde{\mathcal{J}}_N^{(1)}(\mathbf{0}; \lambda) \hat{r}(\mathbf{0})$ , which is of order  $\Gamma$ ; terms such as  $\tilde{\mathcal{J}}_A^{(1)}(\pm\mathbf{u}_l; \lambda) \hat{r}(\mp\mathbf{u}_l)$  are of order  $\Gamma^2$  in general. At the pair-tunneling resonances, however, the  $\tilde{\mathcal{J}}_A^{(1)}(\pm\mathbf{u}_l; \lambda) \hat{r}(\mp\mathbf{u}_l)$  are of order  $\Gamma$  because the  $\hat{r}(\pm\mathbf{u}_l)$  are

of order 1. For the Josephson current we find a similar situation. The only contribution from the first order kernel is  $\tilde{\mathcal{J}}_A^{(1)}(\pm\mathbf{u}_l; \lambda)\hat{r}(\mp\mathbf{u}_l)$ . This is of order  $\Gamma^2$  in general, but of order  $\Gamma$  at the CP resonances.

The second order kernel does not change significantly these estimates. The main contributions to the Josephson current from the second order kernel are of order  $\Gamma^2$  and arise from terms such as  $\tilde{\mathcal{J}}_{AA}^{(2)}[(-1, 1); \lambda]\hat{r}(\mathbf{0})$ . The terms originating from kernels with one anomalous and one normal arc, such as  $\tilde{\mathcal{J}}_{NA}^{(2)}(\pm\mathbf{u}_l; \lambda)\hat{r}(\mp\mathbf{u}_l)$ , only contribute significantly at the pair tunneling resonances, where  $\hat{r}(\mp\mathbf{u}_l)$  is of order 1 and hence they give contributions to the current of order  $\Gamma^2$ . Crucially, these are of order  $\Gamma^3$  elsewhere. Hence, proceeding in this manner allows one to single out all contributions to the current that are at least of order  $\Gamma$  or  $\Gamma^2$ , but also contributions which are of higher order are included. Another example would be  $\tilde{\mathcal{J}}_N^{(1)}(\mathbf{0}; \lambda)\hat{r}[(-1, 1)]$ , which adds to the Josephson current but is  $\propto \Gamma^3$  for  $eV_b \gg \hbar\Gamma$ . Alternatively, the secular approximation [88] can be employed, in which only terms of order  $\Gamma$  and  $\Gamma^2$  are strictly included; we do not consider it in this work.

#### Appendix D: Diagrammatic rules in Liouville space

We summarize the rules needed to translate a given diagram to the expression  $\tilde{\mathcal{K}}_{\dots\psi_i\dots}^{(n)}(\mathbf{m}, \lambda)$ .

1. Draw  $2n$  vertices on a *propagation line*. Associate to the  $K$ th vertex a Liouville index  $\alpha_K$ . In the following,  $K = 0$  is the rightmost vertex and  $K = 2n - 1$  is the leftmost.
2. Draw all possible diagrams where each vertex is linked via a *quasiparticle arc* to another vertex. Discard diagrams which can be cut in two independent diagrams by removing the segment of the propagation line between two vertices without cutting a quasiparticle arc. The  $i$ th quasiparticle arc ( $i = 1, \dots, n$ ) is assigned an energy  $E_i$ , a lead index  $l_i$ , a Fock index  $p_i$ , a spin  $\sigma_i$  and an index  $\psi_i$  which can be either normal (represented by a single arc) or anomalous (double arc).
3. Starting from the rightmost vertex and following the propagation line until the leftmost vertex:
  - (a) For the  $K$ th vertex, if it is the left vertex of the  $i$ th quasiparticle arc, multiply by  $(\alpha_K)^K \mathcal{D}_{\sigma_i}^{\bar{p}_i, \alpha_K}$ ; if it is the right vertex of a normal arc, multiply by  $(\alpha_K)^{K+1} \mathcal{D}_{\sigma_i}^{p_i, \alpha_K}$ ; if it is the right vertex of an anomalous arc, multiply by  $(\alpha_K)^{K+1} \mathcal{D}_{\sigma_i}^{\bar{p}_i, \alpha_K}$ .
  - (b) For the  $J$ th segment of the propagation line between two vertices ( $J = 1, \dots, 2n - 1$ ), mul-

tly by the propagator

$$\frac{1}{\xi_J - i\hbar\mathcal{L}_{QD} + i\hbar\lambda}$$

The  $\xi_J$  of the segment can be determined by conservation of energy in each vertex. Given two segments separated by the *right* vertex of a quasiparticle arc, the energy of the segment to the left must be larger by  $E_i + p_i\psi_i\mu_i$ , where  $\psi_i = +(-)$  for a normal (anomalous) arc. Given two segments separated by the *left* vertex of an arc, the energy of the segment to the right must be larger by  $E_i + p_i\mu_i$ . This is shown in Fig. 8 (a) – (d).

4. For each quasiparticle arc, multiply by  $|t_{l_i}|^2 f(\alpha_K E_i)$ , with  $\alpha_K$  the index of its rightmost vertex. If the arc is normal, multiply by  $G_{N, l_i}(E_i)$ ; if it is anomalous, multiply by  $p_i\sigma_i e^{-ip_i\varphi_i} G_{A, l_i}(E_i) \text{sgn}(E_i)$ . Multiply by  $-1$  for each crossing of two quasiparticle arcs.
5. Sum over the internal (spin) and superoperator indices and integrate over the energies  $E_i$  and multiply by  $1/i\hbar$ . I.e.

$$\frac{1}{i\hbar} \sum_{\{\alpha_K\}} \sum_{\{\sigma_i\}} \int \dots dE_i \dots$$

For each combination of  $\{\psi_i\}, \{l_i\}, \{p_i\}$ , the corresponding diagram is assigned to the kernel  $\tilde{\mathcal{K}}_{\dots\psi_i\dots}^{(n)}(\sum_i \delta_{\psi_i A} p_i \mathbf{u}_i, \lambda)$ .

6. To obtain the contribution to the current kernel, multiply by  $ep_n \delta_{\alpha_{2n-1}, +\ell_n/2}$ , where  $n$  is the leftmost quasiparticle arc and  $\ell_n = (-1)^{\delta_{l_n, L}}$ .

Rule 6 follows from the expression of the symmetrized current operator and the tunneling Liouvillian

$$\mathcal{L}_T = \frac{1}{i\hbar} \sum_{lpk\sigma\alpha} p_{lk}^p C_{l\sigma k}^{p\alpha} \mathcal{D}_{\sigma}^{\bar{p}\alpha}, \quad (\text{D1})$$

$$\hat{I} = \frac{e}{2i\hbar} \sum_{lpk\sigma} \ell_{lk}^p C_{l\sigma k}^{p+} \mathcal{D}_{\sigma}^{\bar{p}+}, \quad (\text{D2})$$

where  $C_{l\sigma k}^{p+} \bullet = \hat{c}_{l\sigma k}^p \bullet$  and  $C_{l\sigma k}^{p-} \bullet = \bullet \hat{c}_{l\sigma k}^p$ .

As an example, let us give the expression for the 3rd order diagram represented in Fig. 8 (e). We first obtain the lead energies in each segment of the propagator line, labeled  $\xi_i$ ,  $i = 1 - 5$  in the diagram. Using Rule 3b we obtain

$$\xi_1 = E_0 + p_0\mu_{l_0}, \quad (\text{D3})$$

$$\xi_2 = E_0 + E_1 + p_0\mu_{l_0} - p_1\mu_{l_1}, \quad (\text{D4})$$

$$\xi_3 = E_0 + p_0\mu_{l_0} - 2p_1\mu_{l_1}, \quad (\text{D5})$$

$$\xi_4 = E_0 + E_2 + p_0\mu_{l_0} - 2p_1\mu_{l_1} + p_2\mu_{l_2}, \quad (\text{D6})$$

$$\xi_5 = E_2 - 2p_1\mu_{l_1} + p_2\mu_{l_2}. \quad (\text{D7})$$

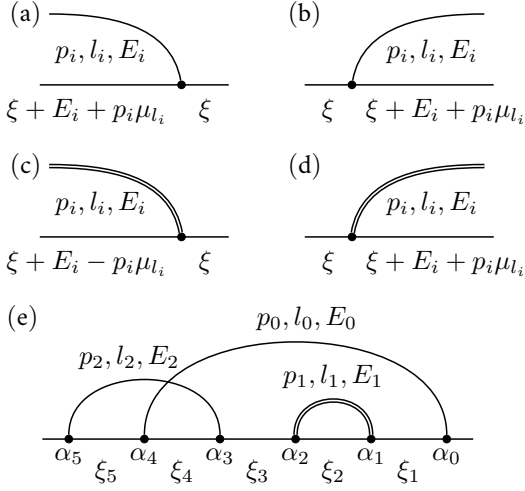


Figure 8. Energy conservation at a vertex (Rule 3b). (a,c) For the right vertex of a quasiparticle arc, add  $E_i + p_i \psi_i \mu_i$ , to the segment to its left, where  $\psi_i = +(-)$  for a normal (anomalous) arc. (b,d) For the left vertex of a quasiparticle arc, remove  $E_i + p_i \mu_i$  from the segment to its left. (e) An exemplary diagram with the energies at every segment written explicitly.

This yields the following contribution

$$\begin{aligned}
& \frac{-1}{i\hbar} \sum_{\{\alpha_K\}_{K=0}^5} \sum_{\{\sigma_i\}_{i=0}^2} \int dE_2 \int dE_1 \int dE_0 \\
& \times \alpha_2 \alpha_0 \sigma_1 p_1 \mathcal{D}_{\sigma_2}^{\bar{p}_2 \alpha_5} \\
& \times \frac{1}{E_2 + p_2 \mu_2 - 2p_1 \mu_1 - i\hbar \mathcal{L}_S + i\hbar \lambda} \mathcal{D}_{\sigma_0}^{\bar{p}_0 \alpha_4} \\
& \times \frac{|t_{l_2}|^2 f(\alpha_3 E_2) G_{N,l_2}(E_2)}{E_2 + p_2 \mu_2 + E_0 + p_0 \mu_0 - 2p_1 \mu_1 - i\hbar \mathcal{L}_{QD} + i\hbar \lambda} \mathcal{D}_{\sigma_2}^{\bar{p}_2 \alpha_3} \\
& \times \frac{1}{E_0 + p_0 \mu_0 - 2p_1 \mu_1 - i\hbar \mathcal{L}_{QD} + i\hbar \lambda} \mathcal{D}_{\sigma_1}^{\bar{p}_1 \alpha_2} \\
& \times \frac{|t_{l_1}|^2 f(\alpha_1 E_1) e^{-ip_1 \varphi_{l_1}} G_{A,l_1}(E_1) \text{sgn}(E_1)}{E_0 + p_0 \mu_0 + E_1 - p_1 \mu_1 - i\hbar \mathcal{L}_{QD} + i\hbar \lambda} \mathcal{D}_{\sigma_1}^{\bar{p}_1 \alpha_1} \\
& \times \frac{|t_{l_0}|^2 f(\alpha_0 E_0) G_{N,l_0}(E_0)}{E_0 + p_0 \mu_0 - i\hbar \mathcal{L}_{QD} + i\hbar \lambda} \mathcal{D}_{\sigma_0}^{\bar{p}_0 \alpha_0}.
\end{aligned}$$

From Rule 2 we see that this belongs to  $\tilde{\mathcal{K}}_{NAN}^{(3)}(p_1 \mathbf{u}_{l_1}, \lambda)$ . The corresponding diagram for the current kernel can be obtained by taking and multiplying by  $ep_2 \ell_2 \delta_{\alpha_5, +/2}$  within the summations.

## Appendix E: First order integrals

The sequential tunneling integral is given by Eq. (44). It can be calculated employing the residue theorem

$$\begin{aligned}
I_{N,l}^q(\nu) &= \int_{-\infty}^{\infty} dE \frac{f(qE) G_{N,l}(E)}{E - \nu + i0^+} \\
&= \lim_{W \rightarrow \infty} \int_{-\infty}^{\infty} dE \frac{f(qE) G_{N,l}(E) L(E, W)}{E - \nu + i0^+}.
\end{aligned} \tag{E1}$$

Here, a Lorentzian cutoff  $L(E, W) = W^2 / (E^2 + W^2)$  has been introduced to regularize the integral for large  $E$ . We introduce also the function

$$g_{N,l}(E) = G_{l,0} \sqrt{\frac{E^2}{E^2 - |\Delta_l|^2}}, \tag{E2}$$

such that  $G_{N,l}(E) = \text{Re}\{g_{N,l}(E)\}$ . We define the analytic continuation of  $g_{N,l}(E)$  having a branch cut at  $\text{Re}\{z\} \in [-|\Delta_l|, |\Delta_l|]$ . In order to calculate  $I_{N,l}^q(\nu)$ , we define the contour  $C_{\pm}$  (sketched in Fig. 9) as a semicircle extending in the upper (lower) half-plane with radius  $R$  and separated by a distance  $\zeta$  from the real axis. In this manner, we have

$$\begin{aligned}
& \int_{-\infty}^{\infty} dE \frac{f(qE) G_{N,l}(E) L(E, W)}{E - \nu + i0^+} \\
&= \lim_{R \rightarrow \infty} \lim_{\zeta \rightarrow 0^+} \sum_{s=\pm} \frac{s}{2} \int_{C_s} dE \frac{f(qE) g_{N,l}(E) L(E, W)}{E - \nu + i0^+}.
\end{aligned} \tag{E3}$$

The integrals over  $C_s$  can be calculated employing the residue theorem. The Fermi function  $f(E)$  has poles at  $iE_k = i\hbar \omega_k$  with residue  $-\beta^{-1}$ , where  $\omega_k = 2\pi i(k + 1/2) / \beta \hbar$ ,  $k \in \mathbb{Z}$  are the Matsubara frequencies. The Lorentzian has poles at  $E = \pm iW$  with residue  $(1/2) (\mp iW)$ . Taking the limits, the integral yields

$$I_{N,l}^q(\nu) = -i\pi f(q\nu) g_{N,l}(\nu - i0^+) \tag{E4}$$

$$-q \left[ \mathcal{S}_{N,l}^{(2)}(\nu) - \lim_{W \rightarrow \infty} \mathcal{C}_{N,l}^{(2)}(W) \right],$$

$$\mathcal{S}_{N,l}^{(2)}(\nu) = \frac{2\pi}{\beta} \sum_{k=0}^{\infty} \frac{E_k g_{N,l}(iE_k)}{E_k^2 + \nu^2}, \tag{E5}$$

$$\begin{aligned}
\mathcal{C}_{N,l}^{(2)}(W) &= \frac{2\pi}{\beta} \sum_{k=0}^{\infty} \frac{1}{2} \left[ \frac{g_{N,l}(iE_k) + g_{N,l}(iW)}{E_k + W} \right] \\
&+ \frac{2\pi}{\beta} \sum_{k=0}^{\infty} \frac{1}{2} \left[ \frac{g_{N,l}(iE_k) - g_{N,l}(iW)}{E_k - W} \right].
\end{aligned} \tag{E6}$$

The infinitesimal factor  $i0^+$  reflects that the function is evaluated below the branch cut. This turns out to be only relevant in the calculation of the imaginary part of  $g_{N,l}(\nu - i0^+)$ . The integral satisfies the property  $I_{N,l}^q(\nu) = -[I_{N,l}^q(-\nu)]^*$ , which guarantees the hermiticity of the density operator.

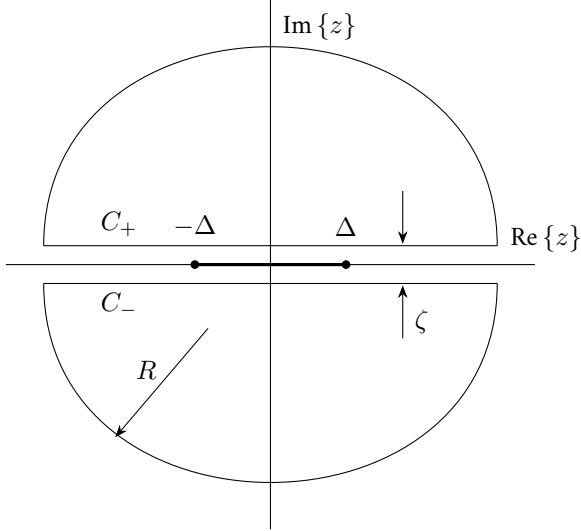


Figure 9. Contours  $C_{\pm}$  for the integration of the sequential tunneling integral  $I_{N,l}^q(\nu)$ . The branch cut of  $g_l(z)$  at  $[-|\Delta_l|, |\Delta_l|]$  are marked by thick lines.

The real valued function  $g_{N,l}(iE)$  is mostly flat except for the region  $|E| \lesssim |\Delta_l|$ , where it exhibits a dip. For  $\beta|\Delta_l| \ll 1$ , the sampling at the Matsubara frequencies ignores the dip and the density of states is effectively flat. In that case, we recover the formula for non-superconducting leads with a flat density of states [89]

$$\lim_{\beta|\Delta_l| \rightarrow 0} S_{N,l}^{(2)}(\nu) = \quad (E7)$$

$$-G_{0,l} \left[ \text{Re} \left\{ \Psi^{(0)} \left( \frac{1}{2} + \frac{i\beta\nu}{2\pi} \right) \right\} + \gamma_{\Psi} \right],$$

$$\lim_{\beta|\Delta_l| \rightarrow 0} C_{N,l}^{(2)}(W) = \quad (E8)$$

$$-G_{0,l} \left[ \text{Re} \left\{ \Psi^{(0)} \left( \frac{1}{2} + \frac{\beta W}{2\pi} \right) \right\} + \gamma_{\Psi} \right],$$

where  $\gamma_{\Psi} = \sum_{k=1}^{\infty} \log(1 + 1/k)$ . Note that the  $C_{N,l}^{(2)}(W) \sim \log \beta W$  encapsulates the logarithmic divergence in the limit  $\beta W \rightarrow \infty$ .

In the opposite (low temperature) limit,  $\beta|\Delta_l| \gg 1$ , the sampling of  $g_{N,l}(iE)$  by the Matsubara energies  $E_k$  is taken as such small intervals that the sum over  $E_k$  can be converted to an integral, with the differential defined as  $\lim_{\beta|\Delta_l| \rightarrow \infty} 2\pi/\beta|\Delta_l|$ . This limit can be performed most conveniently by taking a hard cutoff  $\Theta(W^2 - E^2)$  instead of the Lorentzian in Eq. (E1). Then, employing again the residue theorem and converting the resulting sums to integrals, one obtains

$$\lim_{\beta|\Delta_l| \rightarrow \infty} S_{N,l}^{(2)}(\nu) = \frac{G_{0,l}}{2} \log \frac{\nu^2}{\nu^2 + W^2}. \quad (E9)$$

The equivalent of Eq. (E1) for the anomalous kernel is

given by

$$I_{A,l}^q(\nu) = \int_{-\infty}^{\infty} dE \frac{f(qE) G_{A,l}(E) \text{sgn}(E)}{E - \nu + i0^+}. \quad (E10)$$

Contrary to the normal case, no Lorentzian regularization is needed, since the anomalous DOS decays as  $\sim E^{-1}$  for large  $E$ .

Before proceeding to contour integration, a question arises as to the analytic extension of the  $\text{sgn}(E)$  function. Let us first define the function

$$g_{A,l}(E) = G_{0,l} \sqrt{\frac{|\Delta_l|^2}{E^2 - |\Delta_l|^2}}. \quad (E11)$$

If we choose the branch cut in its analytic continuation to lie in  $\text{Re}\{z\} \in [-|\Delta_l|, |\Delta_l|]$ ,  $g_{A,l}(E)$  has an extra branch cut on the imaginary axis. Fortunately, the branches can be chosen to remove this spurious branch cut. This is equivalent to considering the analytic continuation of  $\text{sgn}(E)$  as  $\text{sgn}(\text{Re}\{E\})$ , which is the natural choice to take. With this, we can proceed as above to find

$$I_{A,l}^q(\nu) = -i\pi f(q\nu) g_{A,l}(\nu - i0^+) \text{sgn}(\nu) - qS_{A,l}^{(2)}(\nu), \quad (E12)$$

$$S_{A,l}^{(2)}(\nu) = \frac{2\pi}{\beta} \sum_{k=0}^{\infty} \frac{i\nu g_{A,l}(iE_k)}{E_k^2 + \nu^2}. \quad (E13)$$

Note that the function  $S_{A,l}^{(2)}(\nu)$  is real, since  $g_{A,l}(i\nu)$  is purely imaginary. The anomalous second order integral satisfies  $I_{A,l}^q(\nu) = [I_{A,l}^q(-\nu)]^*$ . Since  $g_{A,l}(x) \simeq G_{0,l}|\Delta_l|/x$  for  $x \gg |\Delta_l|$ , the Matsubara sum vanishes in the limit  $\beta|\Delta_l| \ll 1$ . In the opposite limit  $\beta|\Delta_l| \gg 1$ , we can transform again the sum into an integral and solve it analytically, yielding

$$\lim_{\beta|\Delta_l| \rightarrow \infty} S_{A,l}^{(2)}(\nu) = g_{A,l}(\nu) \text{sgn}(\nu) \times \text{arctanh} \left[ \lim_{E/|\Delta_l| \rightarrow \infty} \frac{g_{N,l}(iE)}{g_{N,l}(\nu)} \right], \quad (E14)$$

## Appendix F: Second order kernel and integrals

We discuss in detail the second order kernels and discuss the numerical implementation employed to obtain the current and the density operator. We use the notation  $\tilde{\mathcal{K}}_{\psi'\psi}^{(2x)}(\mathbf{m}; \lambda)$ , with  $x \in \{\text{D}, \text{X}\}$  denoting the class of the diagram. Let us consider first the fully normal kernel ( $\psi'\psi = NN$ ). After summing over the lead and Fock

indices of the two lines, the D contribution is given by

$$\begin{aligned} \tilde{\mathcal{K}}_{NN}^{(2D)}(\mathbf{0}; \lambda) &= \frac{1}{i\hbar} \sum_{l'l} \sum_{\sigma'\sigma} \sum_{p'p} \sum_{\{\alpha_i\}} \alpha_3 \alpha_0 \\ &\times |t_{l\nu}|^2 |t_l|^2 \int_{-\infty}^{\infty} dE' \int_{-\infty}^{\infty} dE \mathcal{D}_{\sigma}^{\bar{p}\alpha_3} \\ &\times \frac{G_{N,l'}(E') f(\alpha_1 E')}{E - i\hbar\mathcal{L}_{QD} + p\mu_l + i\hbar\lambda} \mathcal{D}_{\sigma'}^{p'\alpha_2} \\ &\times \frac{1}{E + E' - i\hbar\mathcal{L}_{QD} + p\mu_l + p'\mu_{l'} + i\hbar\lambda} \mathcal{D}_{\sigma'}^{p'\alpha_1} \\ &\times \frac{G_{N,l}(E) f(\alpha_0 E)}{E - i\hbar\mathcal{L}_{QD} + p\mu_l + i\hbar\lambda} \mathcal{D}_{\sigma}^{p\alpha_0}. \end{aligned} \quad (\text{F1})$$

Meanwhile, the fully normal X kernel is given by

$$\begin{aligned} \tilde{\mathcal{K}}_{NN}^{(2X)}(\mathbf{0}; \lambda) &= \frac{-1}{i\hbar} \sum_{l'l} \sum_{\sigma'\sigma} \sum_{p'p} \sum_{\{\alpha_i\}} \alpha_3 \alpha_0 \\ &\times |t_{l\nu}|^2 |t_l|^2 \int_{-\infty}^{\infty} dE' \int_{-\infty}^{\infty} dE \mathcal{D}_{\sigma'}^{\bar{p}'\alpha_3} \\ &\times \frac{G_{N,l'}(E') f(\alpha_1 E')}{E' - i\hbar\mathcal{L}_{QD} + p'\mu_{l'} + i\hbar\lambda} \mathcal{D}_{\sigma}^{\bar{p}\alpha_2} \\ &\times \frac{1}{E + E' - i\hbar\mathcal{L}_{QD} + p\mu_l + p'\mu_{l'} + i\hbar\lambda} \mathcal{D}_{\sigma'}^{p'\alpha_1} \\ &\times \frac{G_{N,l}(E) f(\alpha_0 E)}{E - i\hbar\mathcal{L}_{QD} + p\mu_l + i\hbar\lambda} \mathcal{D}_{\sigma}^{p\alpha_0}. \end{aligned} \quad (\text{F2})$$

For the mixed and anomalous contributions, it suffices to apply the following rules for each normal line that is turned from normal into anomalous, as per the diagrammatic rules. First, the following substitutions are performed:

$$\mathcal{D}_{\sigma_i}^{p_i\alpha_K} \rightarrow \mathcal{D}_{\sigma_i}^{\bar{p}_i\alpha_K}, \quad (\text{F3})$$

$$G_{N,l_i}(E_i) \rightarrow p_i \sigma_i e^{-ip_i \varphi_{l_i}} G_{A,l_i}(E_i) \text{sgn}(E_i), \quad (\text{F4})$$

where the first refers to the rightmost vertex of the quasiparticle line. Then, for each propagator to the left of this vertex, we have to further substitute:

$$i\hbar\mathcal{L}_{QD} \rightarrow i\hbar\mathcal{L}_{QD} + 2p_i \mu_{l_i} / \hbar, \quad (\text{F5})$$

in order to account for Rule 3b of the diagrammatic rules. Finally, the term now contributes to the kernel  $\tilde{\mathcal{K}}(\mathbf{m} + p\mathbf{u}_{l'}; \lambda)$ . For instance, let us turn the two lines of Eq. (F1) from normal to anomalous yields. Now, the terms corresponding for the different values of  $p, l, l'$  will now contribute to distinct kernel components. Using the

rules, we find

$$\begin{aligned} &\tilde{\mathcal{K}}_{AA}^{(2D)}[p(\mathbf{u}_l - \mathbf{u}_{l'}); \lambda] \\ &= \frac{-1}{i\hbar} \sum_{\sigma'\sigma} \sum_{\{\alpha_i\}} \sigma' \sigma \alpha_3 \alpha_0 e^{ip(\varphi_{l'} - \varphi_l)} \\ &\times |t_{l\nu}|^2 |t_l|^2 \int_{-\infty}^{\infty} dE' \int_{-\infty}^{\infty} dE \mathcal{D}_{\sigma}^{\bar{p}\alpha_3} \\ &\times \frac{G_{A,l'}(E') \text{sgn}(E') f(\alpha_1 E')}{E - i\hbar\mathcal{L}_{QD} - p\mu_l + 2p\mu_{l'} + i\hbar\lambda} \mathcal{D}_{\sigma'}^{p\alpha_2} \\ &\times \frac{1}{E + E' - i\hbar\mathcal{L}_{QD} - p\mu_l + p\mu_{l'} + i\hbar\lambda} \mathcal{D}_{\sigma'}^{p\alpha_1} \\ &\times \frac{G_{A,l}(E) \text{sgn}(E) f(\alpha_0 E)}{E - i\hbar\mathcal{L}_{QD} - p\mu_l + i\hbar\lambda} \mathcal{D}_{\sigma}^{\bar{p}\alpha_0}. \end{aligned} \quad (\text{F6})$$

Here we have already taken into account that the only terms that are not zero for the QD Josephson junction have  $p' = \bar{p}$ . The corresponding current kernels are obtained by taking  $\alpha_3 = +$  and multiplying by  $ep'l/2$ .

The integrals that need to be calculated for these kernels have the form

$$I_{\psi'\psi,l'l}^{D,q'q}(\nu, \nu', \Lambda) = \lim_{\eta \rightarrow 0^+} \int_{-\infty}^{\infty} dE' \int_{-\infty}^{\infty} dE \times \quad (\text{F7})$$

$$\frac{f(q'E') G_{\psi',l'}(E')}{E - \nu' + i\eta} \frac{s_{\psi}(E) s_{\psi'}(E')}{E + E' - \Lambda + i\eta} \frac{f(qE) G_{\psi,l}(E)}{E - \nu + i\eta},$$

$$I_{\psi'\psi,l'l}^{X,q'q}(\nu, \nu', \Lambda) = \lim_{\eta \rightarrow 0^+} \int_{-\infty}^{\infty} dE' \int_{-\infty}^{\infty} dE \times \quad (\text{F8})$$

$$\frac{f(q'E') G_{\psi',l'}(E')}{E' - \nu' + i\eta} \frac{s_{\psi}(E) s_{\psi'}(E')}{E + E' - \Lambda + i\eta} \frac{f(qE) G_{\psi,l}(E)}{E - \nu + i\eta},$$

where

$$s_{\psi}(E) = \begin{cases} \text{sgn}(E) & \psi = A, \\ 1 & \psi = N. \end{cases} \quad (\text{F9})$$

Employing partial fraction decomposition, these integrals can be written as

$$I_{\psi'\psi,l'l}^{D,q'q}(\nu, \nu', \Lambda) = \frac{J_{\psi'\psi,l'l}^{q'q}(\nu, \Lambda) - J_{\psi'\psi,l'l}^{q'q}(\nu', \Lambda)}{\nu - \nu'}, \quad (\text{F10})$$

$$\begin{aligned} I_{\psi'\psi,l'l}^{X,q'q}(\nu, \nu', \Lambda) &= I_{\psi',l'}^{q'}(\nu') \frac{I_{\psi,l}^q(\nu) - I_{\psi,l}^q(\Lambda - \nu')}{\nu + \nu' - \Lambda} \\ &\quad - \frac{J_{\psi'\psi,l'l}^{q'q}(\nu, \Lambda) - J_{\psi'\psi,l'l}^{q'q}(\Lambda - \nu', \Lambda)}{\nu + \nu' - \Lambda}, \end{aligned} \quad (\text{F11})$$

where we have defined the function

$$\begin{aligned} J_{\psi',l'l}^{q'q}(\nu, \Lambda) &= \\ &\lim_{\eta \rightarrow 0^+} \int_{-\infty}^{\infty} dE' \int_{-\infty}^{\infty} dE s_{\psi'}(E') s_{\psi}(E) \\ &\times \frac{f(q'E') G_{\psi',l'}(E')}{E - \nu + i\eta} \frac{f(qE) G_{\psi,l}(E)}{E + E' - \Lambda + i\eta}, \end{aligned} \quad (\text{F12})$$

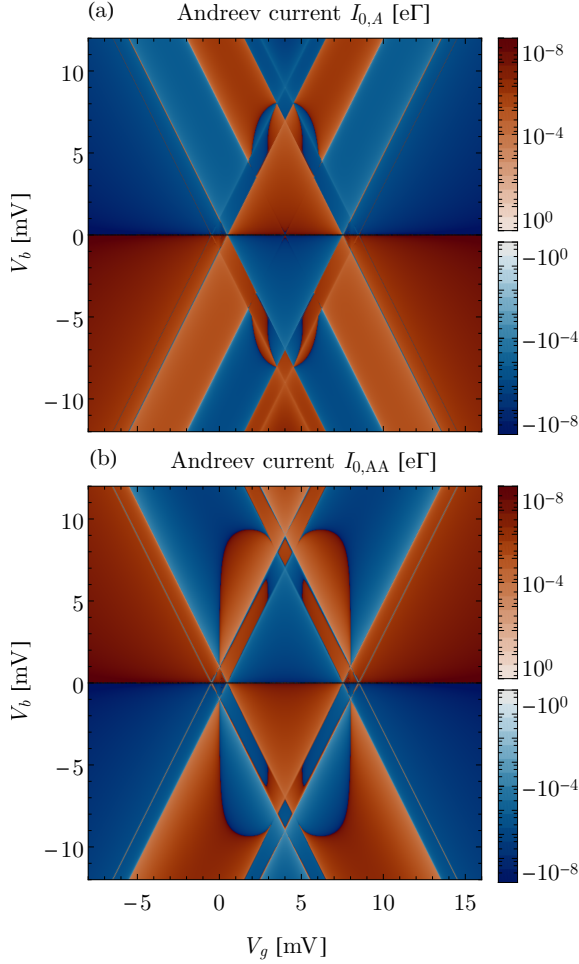


Figure 10. Andreev current components. (a) Andreev current  $I_{0,A}$  originating from the first order kernel as a function of the gate and bias voltages,  $V_g$  and  $V_b$ , respectively, in logarithmic scale for the same parameters as in Fig. 2. (b) Andreev current  $I_{0,AA}$  originating from the second order kernel.

on which we will focus. In the limits  $\nu \rightarrow \nu'$  and  $\Lambda \rightarrow \nu + \nu'$ , the integrals of Eqs. (F10) and (F11) are equal to  $\partial_\nu J_{\psi'\psi, \nu l}^{q'q}(\nu, \Lambda)$  and  $I_{\psi', \nu}^{q'q}(\Lambda - \nu) \partial_\nu I_{\psi, l}^q(\nu) - \partial_\nu J_{\psi'\psi, \nu l}^{q'q}(\nu, \Lambda)$ , respectively.

In order to obtain the results presented in this work, we calculated the integral numerically on a grid and then obtained the derivative through finite differences. Small numerical errors appears when sampling the coherence peaks of the density of states. To help with convergence of the integrals, we consider  $G_{\psi, l}(E) \rightarrow \text{Re}\{g_{\psi, l}(E - i\zeta)\}$  in the grids, and set the Dynes parameter  $\zeta$  accordingly.

Lastly, employing the symmetry properties of this function, in particular

$$J_{\psi'\psi, \nu l}^{q'q}(\nu, \Lambda) = \psi\psi' [J_{\psi'\psi, \nu l}^{q'\bar{q}}(-\nu, -\Lambda)]^*, \quad (\text{F13})$$

with the shorthand notation  $\psi \equiv (-1)^{\delta_{\psi, A}}$ , it is possible to reduce the number of calculated grids by half. Even then, eight grids need to be calculated in the case of identical gaps for both leads, and four times that number for different gaps. Fortunately, Eq. (F12) can be reduced to one-dimensional integrals by solving for the variable  $E'$  using the expression for the sequential tunneling integral given above.

### Appendix G: Contributions to the Andreev current

We discuss separately the two contributions to the Andreev current,  $I_{0,A}$  and  $I_{0,AA}$ , which are represented in Fig. 10. We first point out that the two terms cancel inside the Coulomb diamonds almost exactly. This signals that the Andreev current is, outside of the resonances, intrinsically a second order process and that these two contributions must be understood together. We say here “almost exactly” because higher order contributions such as those discussed in Section IV B result in small differences. This can be appreciated here for the pair tunneling resonances close to  $eV_b = 0, eV_g = 4$  mV, where  $I_{0,A}$  shows a change in the current that is not observed in  $I_{0,AA}$ .

For  $I_{0,A}$  we observe that the current changes sign close to but not exactly at the resonances, where the current is actually finite, as can be seen in Fig. 2 (c). For  $I_{0,AA}$ , we see the vertical features for  $eV_g = 0, U$ , which appeared as dips in the differential conductance in Fig. 2. For  $eV_g = 0$  we can study this feature employing an infinite interaction approximation to the Andreev current. Provided that  $\mu_l \ll U$ , we find

$$\lim_{U \rightarrow \infty} I_{0,AA} = 2e \sum_l \ell \Gamma_l^2 \frac{1}{\mu_l} \frac{\hbar}{2\pi} \quad (\text{G1})$$

$$\times G_{A,l}(\mu_l) \text{sgn}(\mu_l) S_{A,l}^{(2)}(\mu_l) [f(\mu_l) p_1/2 - f(-\mu_l) p_0],$$

where  $p_0 = \langle 0 | \hat{r}(\mathbf{0}) | 0 \rangle$  is the population of the unoccupied state and  $p_1 = \sum_\sigma p_\sigma$  with  $p_\sigma = \langle \sigma | \hat{r}(\mathbf{0}) | \sigma \rangle$ . For  $eV_b > \Delta$ , along the vertical line  $eV_g = 0$  in the stability diagram  $p_1 = 2p_0$  due to symmetry, and we find

$$\lim_{U \rightarrow \infty} I_{0,AA} = -2e \sum_l \ell \Gamma_l^2 \frac{1}{2\ell e V_b} \frac{\hbar}{2\pi}$$

$$\times G_{A,l}(\ell e V_b) \text{sgn}(\ell e V_b) S_{A,l}^{(2)}(\ell e V_b) \tanh(\ell \beta e V_b/2).$$

Since  $S_{A,l}^{(2)}(\nu)$  is odd in  $\nu$ , [see Eq. (E13)], for equal tunneling rates  $\Gamma_l \equiv \Gamma$  and absolute values of the gap  $|\Delta_l| \equiv \Delta$ , the sum over the two leads cancels and the Andreev current is zero. This can be seen clearly in Fig. 10 (b) for  $\Delta < eV_b \ll U$ . For  $eV_g = U$ , the analysis is the same due to particle-hole symmetry around  $eV_g = U/2$ .

We also remark the absence of features along the pair tunneling resonances for  $I_{0,AA}$ , which as pointed out above originate exclusively from  $I_{0,A}$ .

- 
- [1] J. C. Cuevas, A. Martín-Rodero, and A. L. Yeyati, Hamiltonian approach to the transport properties of superconducting quantum point contacts, *Phys. Rev. B* **54**, 7366 (1996).
- [2] J. C. Cuevas, J. Heurich, A. Martín-Rodero, A. Levy Yeyati, and G. Schön, Subharmonic shapiro steps and assisted tunneling in superconducting point contacts, *Phys. Rev. Lett.* **88**, 157001 (2002).
- [3] A. A. Golubov, M. Y. Kupriyanov, and E. Il'ichev, The current-phase relation in josephson junctions, *Rev. Mod. Phys.* **76**, 411 (2004).
- [4] L. Bretheau, C. O. Girit, C. Urbina, D. Esteve, and H. Pothier, Supercurrent spectroscopy of andreev states, *Phys. Rev. X* **3**, 041034 (2013).
- [5] Y. Oreg, G. Refael, and F. von Oppen, Helical liquids and majorana bound states in quantum wires, *Phys. Rev. Lett.* **105**, 10.1103/physrevlett.105.177002 (2010).
- [6] A. Cook and M. Franz, Majorana fermions in a topological-insulator nanowire proximity-coupled to an *s*-wave superconductor, *Phys. Rev. B* **84**, 201105 (2011).
- [7] T. D. Stanescu and S. Tewari, Majorana fermions in semiconductor nanowires: fundamentals, modeling, and experiment, *Journal of Physics: Condensed Matter* **25**, 233201 (2013).
- [8] Y. Tokura and N. Nagaosa, Nonreciprocal responses from non-centrosymmetric quantum materials, *Nature Communications* **9**, 10.1038/s41467-018-05759-4 (2018).
- [9] C. Baumgartner, L. Fuchs, A. Costa, S. Reinhardt, S. Gronin, G. C. Gardner, T. Lindemann, M. J. Manfra, P. E. F. Junior, D. Kochan, J. Fabian, N. Paradiso, and C. Strunk, Supercurrent rectification and magnetochiral effects in symmetric josephson junctions, *Nature Nanotechnology* **17**, 39 (2021).
- [10] C. Baumgartner, L. Fuchs, A. Costa, J. Picó-Cortés, S. Reinhardt, S. Gronin, G. C. Gardner, T. Lindemann, M. J. Manfra, P. E. F. Junior, D. Kochan, J. Fabian, N. Paradiso, and C. Strunk, Effect of rashba and dresselhaus spin-orbit coupling on supercurrent rectification and magnetochiral anisotropy of ballistic josephson junctions, *Journal of Physics: Condensed Matter* **34**, 154005 (2022).
- [11] A. H. Pfeffer, J. E. Duvauchelle, H. Courtois, R. Mélin, D. Feinberg, and F. Lefloch, Subgap structure in the conductance of a three-terminal josephson junction, *Phys. Rev. B* **90**, 075401 (2014).
- [12] J. S. Meyer and M. Houzet, Nontrivial chern numbers in three-terminal josephson junctions, *Phys. Rev. Lett.* **119**, 136807 (2017).
- [13] Y.-J. Doh, J. A. van Dam, A. L. Roest, E. P. A. M. Bakkers, L. P. Kouwenhoven, and S. D. Franceschi, Tunable supercurrent through semiconductor nanowires, *Science* **309**, 272 (2005).
- [14] J.-P. Cleuziou, W. Wernsdorfer, V. Bouchiat, T. Ondaçuhu, and M. Monthieux, Carbon nanotube superconducting quantum interference device, *Nature Nanotechnology* **1**, 53 (2006).
- [15] J.-D. Pillet, C. H. L. Quay, P. Morfin, C. Bena, A. L. Yeyati, and P. Joyez, Andreev bound states in supercurrent-carrying carbon nanotubes revealed, *Nature Physics* **6**, 965 (2010).
- [16] T. Dirks, T. L. Hughes, S. Lal, B. Uchoa, Y.-F. Chen, C. Chialvo, P. M. Goldbart, and N. Mason, Transport through andreev bound states in a graphene quantum dot, *Nature Physics* **7**, 386 (2011).
- [17] R. Delagrange, D. J. Luitz, R. Weil, A. Kasumov, V. Meden, H. Bouchiat, and R. Deblock, Manipulating the magnetic state of a carbon nanotube josephson junction using the superconducting phase, *Phys. Rev. B* **91**, 241401 (2015).
- [18] F. Siano and R. Egger, Josephson current through a nanoscale magnetic quantum dot, *Phys. Rev. Lett.* **93**, 047002 (2004).
- [19] G. Sellier, T. Kopp, J. Kroha, and Y. S. Barash,  $\pi$  junction behavior and andreev bound states in kondo quantum dots with superconducting leads, *Phys. Rev. B* **72**, 174502 (2005).
- [20] C. Karrasch, A. Oguri, and V. Meden, Josephson current through a single anderson impurity coupled to bcs leads, *Phys. Rev. B* **77**, 024517 (2008).
- [21] N. M. Chtchelkatchev and Y. V. Nazarov, Andreev quantum dots for spin manipulation, *Phys. Rev. Lett.* **90**, 226806 (2003).
- [22] M. Hays, V. Fatemi, D. Bouman, J. Cerrillo, S. Diamond, K. Serniak, T. Connolly, P. Krogstrup, J. Nygard, A. Levy Yeyati, A. Geresdi, and M. H. Devoret, Coherent manipulation of an andreev spin qubit, *Science* **373**, 430 (2021).
- [23] A. Martín-Rodero and A. L. Yeyati, Josephson and andreev transport through quantum dots, *Advances in Physics* **60**, 899 (2011).
- [24] V. Meden, The anderson-josephson quantum dot—a theory perspective, *Journal of Physics: Condensed Matter* **31**, 163001 (2019).
- [25] J. A. van Dam, Y. V. Nazarov, E. P. A. M. Bakkers, S. D. Franceschi, and L. P. Kouwenhoven, Supercurrent reversal in quantum dots, *Nature* **442**, 667 (2006).
- [26] H. I. Jørgensen, T. Novotný, K. Grove-Rasmussen, K. Flensberg, and P. E. Lindelof, Critical current  $0-\pi$  transition in designed josephson quantum dot junctions, *Nano Letters* **7**, 2441 (2007).
- [27] R. Maurand, T. Meng, E. Bonet, S. Florens, L. Marty, and W. Wernsdorfer, First-order  $0-\pi$  quantum phase transition in the kondo regime of a superconducting carbon-nanotube quantum dot, *Phys. Rev. X* **2**, 011009 (2012).

- [28] R. Delagrangé, R. Weil, A. Kasumov, M. Ferrer, H. Bouchiat, and R. Deblock,  $0-\pi$  quantum transition in a carbon nanotube Josephson junction: Universal phase dependence and orbital degeneracy, *Phys. Rev. B* **93**, 195437 (2016).
- [29] X. Li, E. Barnes, J. P. Kestner, and S. Das Sarma, Intrinsic errors in transporting a single-spin qubit through a double quantum dot, *Phys. Rev. A* **96**, 012309 (2017).
- [30] A. Eichler, R. Deblock, M. Weiss, C. Karrasch, V. Meden, C. Schönenberger, and H. Bouchiat, Tuning the Josephson current in carbon nanotubes with the Kondo effect, *Phys. Rev. B* **79**, 161407 (2009).
- [31] R. S. Deacon, Y. Tanaka, A. Oiwa, R. Sakano, K. Yoshida, K. Shibata, K. Hirakawa, and S. Tarucha, Tunneling spectroscopy of Andreev energy levels in a quantum dot coupled to a superconductor, *Phys. Rev. Lett.* **104**, 076805 (2010).
- [32] J.-D. Pillet, P. Joyez, R. Žitko, and M. F. Goffman, Tunneling spectroscopy of a single quantum dot coupled to a superconductor: From Kondo ridge to Andreev bound states, *Phys. Rev. B* **88**, 045101 (2013).
- [33] A. Bargerbos, M. Pita-Vidal, R. Žitko, J. Ávila, L. J. Splitthoff, L. Grünhaupt, J. J. Wesdorp, C. K. Andersen, Y. Liu, L. P. Kouwenhoven, R. Aguado, A. Kou, and B. van Heck, Singlet-doublet transitions of a quantum dot Josephson junction detected in a transmon circuit, *PRX Quantum* **3**, 030311 (2022).
- [34] A. V. Rozhkov and D. P. Arovas, Josephson coupling through a magnetic impurity, *Phys. Rev. Lett.* **82**, 2788 (1999).
- [35] A. Martín-Rodero and A. L. Yeyati, The Andreev states of a superconducting quantum dot: mean field versus exact numerical results, *Journal of Physics: Condensed Matter* **24**, 385303 (2012).
- [36] A. A. Clerk and V. Ambegaokar, Loss of  $\pi$ -junction behavior in an interacting impurity Josephson junction, *Phys. Rev. B* **61**, 9109 (2000).
- [37] E. Vecino, A. Martín-Rodero, and A. L. Yeyati, Josephson current through a correlated quantum level: Andreev states and  $\pi$  junction behavior, *Phys. Rev. B* **68**, 035105 (2003).
- [38] S. D. Franceschi, L. Kouwenhoven, C. Schönenberger, and W. Wernsdorfer, Hybrid superconductor–quantum dot devices, *Nature Nanotechnology* **5**, 703 (2010).
- [39] L. I. Glazman and K. A. Matveev, Resonant Josephson current through Kondo impurities in a tunnel barrier, *Soviet Journal of Experimental and Theoretical Physics Letters* **49**, 659 (1989).
- [40] M.-S. Choi, C. Bruder, and D. Loss, Spin-dependent Josephson current through double quantum dots and measurement of entangled electron states, *Phys. Rev. B* **62**, 13569 (2000).
- [41] T. Novotný, A. Rossini, and K. Flensberg, Josephson current through a molecular transistor in a dissipative environment, *Phys. Rev. B* **72**, 224502 (2005).
- [42] H. Schoeller and G. Schön, Mesoscopic quantum transport: Resonant tunneling in the presence of a strong Coulomb interaction, *Phys. Rev. B* **50**, 18436 (1994).
- [43] J. König, H. Schoeller, and G. Schön, Zero-bias anomalies and boson-assisted tunneling through quantum dots, *Phys. Rev. Lett.* **76**, 1715 (1996).
- [44] J. König, J. Schmid, H. Schoeller, and G. Schön, Resonant tunneling through ultrasmall quantum dots: Zero-bias anomalies, magnetic-field dependence, and boson-assisted transport, *Phys. Rev. B* **54**, 16820 (1996).
- [45] J. Kern and M. Grifoni, Transport across an Anderson quantum dot in the intermediate coupling regime, *The European Physical Journal B* **86**, 10.1140/epjb/e2013-40618-9 (2013).
- [46] L. Magazzù and M. Grifoni, Feynman-Vernon influence functional approach to quantum transport in interacting nanojunctions: An analytical hierarchical study, *Phys. Rev. B* **105**, 125417 (2022).
- [47] A. Donarini and M. Grifoni, *Quantum Transport in Interacting Nanojunctions* (Springer, 2024).
- [48] R. B. Saptsov and M. R. Wegewijs, Fermionic superoperators for zero-temperature nonlinear transport: Real-time perturbation theory and renormalization group for Anderson quantum dots, *Phys. Rev. B* **86**, 235432 (2012).
- [49] M. G. Pala, M. Governale, and J. König, Nonequilibrium Josephson and Andreev current through interacting quantum dots, *New Journal of Physics* **9**, 278 (2007).
- [50] M. Governale, M. G. Pala, and J. König, Real-time diagrammatic approach to transport through interacting quantum dots with normal and superconducting leads, *Physical Review B* **77**, 10.1103/physrevb.77.134513 (2008).
- [51] A. G. Moghaddam, M. Governale, and J. König, Driven superconducting proximity effect in interacting quantum dots, *Phys. Rev. B* **85**, 094518 (2012).
- [52] P. Recher, E. V. Sukhorukov, and D. Loss, Andreev tunneling, Coulomb blockade, and resonant transport of nonlocal spin-entangled electrons, *Phys. Rev. B* **63**, 165314 (2001).
- [53] B. Probst, F. Domínguez, A. Schroer, A. L. Yeyati, and P. Recher, Signatures of nonlocal Cooper-pair transport and of a singlet-triplet transition in the critical current of a double-quantum-dot Josephson junction, *Phys. Rev. B* **94**, 155445 (2016).
- [54] R. Hussein, L. Jaurigue, M. Governale, and A. Braggio, Double quantum dot Cooper-pair splitter at finite couplings, *Phys. Rev. B* **94**, 235134 (2016).
- [55] R. Hussein, M. Governale, S. Kohler, W. Belzig, F. Giazotto, and A. Braggio, Nonlocal thermoelectricity in a Cooper-pair splitter, *Phys. Rev. B* **99**, 075429 (2019).
- [56] A. Kumar, M. Gaim, D. Steininger, A. L.

- Yeyati, A. Martín-Rodero, A. K. Hüttel, and C. Strunk, Temperature dependence of andreev spectra in a superconducting carbon nanotube quantum dot, *Phys. Rev. B* **89**, 075428 (2014).
- [57] G. Kiršanskas, M. Goldstein, K. Flensberg, L. I. Glazman, and J. Paaske, Yu-shiba-rusinov states in phase-biased superconductor–quantum dot–superconductor junctions, *Phys. Rev. B* **92**, 235422 (2015).
- [58] J. Eldridge, M. G. Pala, M. Governale, and J. König, Superconducting proximity effect in interacting double-dot systems, *Phys. Rev. B* **82**, 184507 (2010).
- [59] B. Sothmann, S. Weiss, M. Governale, and J. König, Unconventional superconductivity in double quantum dots, *Phys. Rev. B* **90**, 220501 (2014).
- [60] B. Sothmann and R. P. Tiwari, Josephson response of a conventional and a noncentrosymmetric superconductor coupled via a double quantum dot, *Phys. Rev. B* **92**, 014504 (2015).
- [61] D. Futterer, J. Swiebodzinski, M. Governale, and J. König, Renormalization effects in interacting quantum dots coupled to superconducting leads, *Phys. Rev. B* **87**, 014509 (2013).
- [62] L. C. Ortmanns, M. R. Wegewijs, and J. Splettstoesser, Solution of master equations by fermionic-duality: Time-dependent charge and heat currents through an interacting quantum dot proximized by a superconductor, *SciPost Physics* **14**, 10.21468/scipost-phys.14.5.095 (2023).
- [63] L. C. Ortmanns, J. Splettstoesser, and M. R. Wegewijs, Transient transport spectroscopy of an interacting quantum dot proximized by a superconductor: Charge and heat currents after a switch, *Phys. Rev. B* **108**, 085426 (2023).
- [64] L. Dell’Anna, A. Zazunov, and R. Egger, Superconducting nonequilibrium transport through a weakly interacting quantum dot, *Phys. Rev. B* **77**, 104525 (2008).
- [65] T. Jonckheere, A. Zazunov, K. V. Bayandin, V. Shumeiko, and T. Martin, Nonequilibrium supercurrent through a quantum dot: Current harmonics and proximity effect due to a normal-metal lead, *Phys. Rev. B* **80**, 184510 (2009).
- [66] B. M. Andersen, K. Flensberg, V. Koerting, and J. Paaske, Nonequilibrium transport through a spinful quantum dot with superconducting leads, *Phys. Rev. Lett.* **107**, 256802 (2011).
- [67] B. Hiltcher, M. Governale, and J. König, ac josephson transport through interacting quantum dots, *Phys. Rev. B* **86**, 235427 (2012).
- [68] J. F. Rentrop, S. G. Jakobs, and V. Meden, Nonequilibrium transport through a josephson quantum dot, *Phys. Rev. B* **89**, 235110 (2014).
- [69] B. Lamic, J. S. Meyer, and M. Houzet, Josephson radiation in a superconductor-quantum dot-superconductor junction, *Phys. Rev. Res.* **2**, 033158 (2020).
- [70] D. Watfa, R. Delagrangé, A. Kadlecová, M. Ferrier, A. Kasumov, H. Bouchiat, and R. Deblock, Collapse of the josephson emission in a carbon nanotube junction in the kondo regime, *Phys. Rev. Lett.* **126**, 126801 (2021).
- [71] B. D. Josephson, Possible new effects in superconductive tunnelling, *Physics Letters* **1**, 251 (1962).
- [72] J. Siegl, J. Picó-Cortés, and M. Grifoni, Particle conserving approach to ac-dc driven interacting quantum dots with superconducting leads, *Phys. Rev. B* **107**, 115405 (2023).
- [73] R. E. Harris, Cosine and other terms in the josephson tunneling current, *Phys. Rev. B* **10**, 84 (1974).
- [74] J. R. Waldram, The josephson effects in weakly coupled superconductors, *Reports on Progress in Physics* **39**, 751 (1976).
- [75] R. S. Deacon, J. Wiedenmann, E. Bocquillon, F. Domínguez, T. M. Klapwijk, P. Leubner, C. Brüne, E. M. Hankiewicz, S. Tarucha, K. Ishibashi, H. Buhmann, and L. W. Molenkamp, Josephson radiation from gapless andreev bound states in hgte-based topological junctions, *Phys. Rev. X* **7**, 021011 (2017).
- [76] A. J. Leggett, *Quantum Liquids: Bose Condensation and Cooper Pairing in Condensed-Matter Systems (Oxford Graduate Texts)* (Oxford University Press, 2006).
- [77] J. Picó-Cortés, *AC dynamics of quantum dots and Josephson junctions for quantum technologies*, Ph.D. thesis, Universidad Autónoma de Madrid (2021).
- [78] M. Tinkham, *Introduction to Superconductivity: Second Edition (Dover Books on Physics)* (Dover Publications, 2004).
- [79] S. Pfaller, A. Donarini, and M. Grifoni, Subgap features due to quasiparticle tunneling in quantum dots coupled to superconducting leads, *Phys. Rev. B* **87**, 155439 (2013).
- [80] S. Nakajima, On quantum theory of transport phenomena: Steady diffusion, *Progress of Theoretical Physics* **20**, 948 (1958).
- [81] R. Zwanzig, Ensemble method in the theory of irreversibility, *The Journal of Chemical Physics* **33**, 1338 (1960).
- [82] C. Bruder and H. Schoeller, Charging effects in ultrasmall quantum dots in the presence of time-varying fields, *Phys. Rev. Lett.* **72**, 1076 (1994).
- [83] B. D. Josephson, Coupled superconductors, *Rev. Mod. Phys.* **36**, 216 (1964).
- [84] B. D. Josephson, Supercurrents through barriers, *Advances in Physics* **14**, 419 (1965).
- [85] K. Grove-Rasmussen, H. I. Jørgensen, B. M. Andersen, J. Paaske, T. S. Jespersen, J. Nygård, K. Flensberg, and P. E. Lindelof, Superconductivity-enhanced bias spectroscopy in carbon nanotube quantum dots, *Phys. Rev. B* **79**, 134518 (2009).
- [86] S. Ratz, A. Donarini, D. Steininger, T. Geiger, A. Kumar, A. K. Hüttel, C. Strunk, and M. Grifoni, Thermally induced subgap features in the cotunneling spectroscopy of a carbon nanotube, *New Journal of Physics* **16**, 123040

- (2014).
- [87] G. Johansson, E. N. Bratus, V. S. Shumeiko, and G. Wendin, Resonant multiple andreev reflections in mesoscopic superconducting junctions, *Phys. Rev. B* **60**, 1382 (1999).
- [88] S. Koller, M. Grifoni, M. Leijnse, and M. R. Wegewijs, Density-operator approaches to transport through interacting quantum dots: Simplifications in fourth-order perturbation theory, *Phys. Rev. B* **82**, 235307 (2010).
- [89] S. Koller, *Spin phenomena and higher order effects in transport across interacting quantum-dots*, *Ph.D. thesis*, University of Regensburg (2010).